Thermo-Metallo-Mechanical Modelling of Heat Treatment Induced Residual Stress in Ti-6Al-4V Alloy

W. Rae[1]*

[1]*Advanced Forming Research Centre (AFRC), University of Strathclyde, 85 Inchinnan Drive, Glasgow, UK*

*william.rae@strath.ac.uk

https://orcid.org/0000-0002-7514-2359

Thermo-Metallo-Mechanical Modelling of Heat Treatment Induced Residual Stress in Ti-6Al-4V Alloy

Residual stress fields dynamically fluctuate throughout the manufacturing process of metallic components and are caused by local misfit of a thermal, mechanical or metallurgical nature. Recent advances have been made in the area of microstructure and residual stress prediction; yet few have considered dual-phase titanium alloys. The aim of the work presented was to carry out a review of the existing state-of-the-art in residual stress modelling with an intended application to industrial heat treatment of Ti-6Al-4V alloy. Four areas were evaluated: thermal, mechanical and metallurgical sub-models, and model validation *via* residual stress measurement. Recommendations for future research include further investigation of transformation induced plasticity and stress relaxation behaviour in Ti-6Al-4V.

Keywords: residual stress; titanium alloys; Ti-6Al-4V; phase transformation; numerical simulation; heat treatment; stress relaxation

1. Introduction

Titanium and its alloys are often within selected for use in high-value structural components in a number of applications due to their favourable strength-to-weight ratio, superior corrosion resistance and excellent mechanical properties [1]. The aerospace industry accounts for the majority of global titanium consumption – over 80% – which is used to produce a number of alloys; of which Ti-6Al-4V is the most widespread variant [2]. The main applications of these alloys include the airframe, landing gear, low pressure compressor components and fan blades within gas turbine engines; with increasing numbers of critical components utilising the alloy [2].

The material is commonly subjected to a prescribed set of thermal and thermo-mechanical cycles to realize a final microstructure which exhibits favourable mechanical properties, yet residual stress must be taken into account and adequately controlled to

ensure optimal performance. Understanding the origin of residual stresses and their evolution throughout the manufacturing process is a key challenge faced by those in industry. The inclusion of tensile residual stress can reduce fatigue life and lead to cracking, and high magnitudes of residual stress can cause deviations from dimensional tolerances during machining operations [3]. Therefore it is important to develop an understanding of such stresses in order to reliably predict and control processes to achieve a final part with the desired operational performance without need for rework [4]. Thus, if accurate predictive models for evolution of microstructure and residual stress can be developed and adopted by industry, this could reduce the need for trial-and-error based approaches which may allow for improved material performance whilst minimising production costs [4, 5].

Residual stresses exist in all manufactured components to some extent. They can be thought of as internal stresses which remain in a part when it is no longer subjected to any external forces. These residual stresses can be induced by plastic deformation, thermal fluctuations, phase transformation or any micro- and macro- mechanisms that results in a form of misfit within a part [6]. Therefore residual stresses are often produced as a result of metalworking operations as most of these mechanisms are active [3]. Residual stress fields act across differing length scales. These are characterised as: type I macro-stress which varies over large distances comparable to the dimensions of the part, type II intergranular stress which varies over the grain scale, and type III atomic scale stress [7]. For the purposes of manufacturing large scale metallic engineering components, type I macro-stresses are generally of most importance and are therefore the main concern in industrial process modelling endeavours [7].

A number of works have been conducted whereby finite element analysis has been employed to model the evolution of residual stress during thermo-mechanical processing in steel [4, 8, 9], aluminium alloys [10, 11, 12, 13] and nickel-based superalloys [14, 15]. Model development has been ongoing since the late 1950's whereby Weiner and Huddleston [16] conducted computer-assisted simulation of residual stress in heat treated steel cylinders. However, there is a clear lack of published literature surrounding the modelling of residual stress evolution in titanium alloys; particularly involving the heat treatment of Ti-6Al-4V alloy [17]. The few studies which have been conducted largely concern additive manufacturing and welding and tend to simplify or omit the effect of metallurgical influences on residual stress [18, 19, 20]. Yet thermal, metallurgical and mechanical influences are inextricably linked to the evolution of residual stress and must be considered accordingly [6].

The aim of the work presented was to carry out a review of the existing state-of-the-art in residual stress modelling with an intended application to industrial heat treatment of Ti-6Al-4V alloy. It was desired to understand the limitations of existing knowledge of the subject matter and identify areas for future work.

Titanium Alloy Ti-6Al-4V

Elemental titanium exhibits the highest strength-to-weight ratio of any metallic element, as well as excellent corrosion resistance and great high temperature mechanical properties [21]. Pure titanium displays a hexagonal close packed (hcp) crystal structure; known as α titanium, at low temperatures [22]. However, an allotropic phase transformation occurs upon heating to above 882°C. This produces a body-centred cubic (bcc) structure known as β titanium [22]. This transition temperature is called the β-transus temperature. The crystallographic orientation relationship between the α and β phase is described by the Burgers relationship [23] which states that 12 distinct α variants may be developed within

each β grain. Yet each variant is not represented proportionally, leading to distinct crystallographic textures due to a phenomena called variant selection [24, 25].

The addition of alloying elements, vanadium and aluminium, in Ti-6Al-4V lead to an alloy with an increased β-transus, yet stable α and β phases at room temperature. The ASTM standard specification for the allowable chemical composition of Ti-6Al-4V alloy in billet and bar form is shown in Table 1 [26]. The addition of aluminium leads to reduced alloy density whilst strengthening the α phase and increasing the β-transus temperature [27]. On the other hand, the inclusion of vanadium improves hot workability and reduces the β-transus whilst also promoting stability of the β phase at room temperature [27]. This is illustrated as binary phase diagrams in Fig. 1 [28, 29]. A β-transus of 995±15°C is exhibited by Ti-6Al-4V [22, 30]. The onset of the α→β transformation has been identified at approximately 550°C [31] , whilst the β→α transformation begins when cooling below the β-transus and is further discussed within as part of the metallurgical sub-model . The fraction of retained β phase at room temperature is not only dependent on alloying elements, but also thermal history, and can range from 0 to 12 vol% [32, 33]. Elemental diffusion, predominantly of vanadium, upon cooling drives the growth of the α phase and causes preferential partitioning of solutes in the α and β phase [34]. The effect of this has been quantified by Elmer *et al*. [33] who found 7% Al and 1% V in α, with 3% Al and 15% V in β at room temperature [1].

A selection of typical bulk material properties exhibited by Ti-6Al-4V are compared against that of high purity titanium (> 99.98 wt% Ti) in Table 2. From Table 2 it is apparent that Ti-6Al-4V exhibits a superior strength-to-density ratio in comparison with its unalloyed counterpart. However, the ambient properties of Ti-6Al-4V alloy are

[1] Values expressed in wt%

also highly dependent on the microstructure which is influenced by thermo-mechanical processing and heat treatment [17]. For example, high cooling rates experienced during water quenching (~10,000°C/min) from above the β-transus can lead to a yield strength of 1100 MPa whereas a value of 850 MPa may be exhibited after slow furnace cooling (<100°C/min) [35, 36]. Similarly, ultimate tensile strength, creep resistance, fatigue strength and ductility are particularly influenced by process history [27, 35, 37, 38]. This must be taken into consideration when using literature data for process modelling and when evaluating magnitudes of residual stress [39].

Figure 1: Binary phase diagrams of major alloying elements, aluminium (a), and vanadium (b), present in Ti-6Al-4V [28, 29].

Table 1: ASTM B348-13 Standard Specification for the composition of Ti-6Al-4V Grade 5 alloy [26].

Element Content (wt%)							
Al	V	Fe	O	C	N	H	Ti
5.5-6.75	3.5-4.5	< 0.4	< 0.2	< 0.08	< 0.05	< 0.00125	Bal.

Table 2: Comparison of selected bulk properties of high purity Ti and Ti-6Al-4V [22, 40].

Property	**High Purity Ti (> 99.98 wt%)**	**Ti-6Al-4V**
Density (g/cc)	4.51	4.43
Young's Modulus (GPa)	100-145	110-140
Yield Strength (MPa)	140	800-1100
Ultimate Tensile Strength (MPa)	235	950
Poisson's Ratio	0.32	0.342
Beta Transus Temperature (°C)	882	995±15

Heat Treatment of Ti-6Al-4V

Ti-6Al-4V alloy is initially produced by crushing and melting titanium sponge and adding the necessary alloying elements to the melt [1]. The melted alloy is then cast to produce an ingot which is the base geometry for thermo-mechanical processing and machining.

The ingot is usually firstly annealed within the β phase field, this process is called homogenization; producing a uniform globularised microstructure with good workability [40]. This is followed by plastic deformation at a temperature either within the α+β or β phase field dependant on the desired final microstructure. Bulk metalforming processes such as forging or rolling may be utilised in order to carry out this deformation.

Following metalforming, a combination of successive heat treatment cycles may be applied to the material to achieve the desired mechanical properties. The two most common heat treatment processes are annealing and solution treatment and aging (STA) [41]. The microstructural evolution due to such heat treatment processes is heavily dependent on the temperature at which the heat treatment is conducted, as well as the 'soak duration', and the subsequent cooling rate [27, 42, 43]. Additionally, thermo-mechanical processing can alter the magnitude and distribution of type I, II and III residual stress throughout the material [6]. Typically, mechanically induced residual stress is considered to act across the type I scale, whilst thermal gradients act across both the type I and II scales, and transformation induced stress is of type II yet may average to a non-zero value over the macro-scale [7]. These residual stresses may be intensified or mitigated, depending on the particular thermo-mechanical process conditions employed.

Solution treatment is often used after deformation to obtain a material with high strength and reasonable ductility [36]. It is conducted at temperatures high in the α+β phase field; producing a bimodal microstructure of α in a transformed β matrix, or in the β phase field; producing a lamellar 'β–annealed' microstructure [21, 35]. Water may be

used as a quenchant in order to minimise diffusion of atoms within the solid solution. However, this leads to increased differential thermal gradients in the material; associated with a generation of high magnitudes of residual stress. Aging may then be completed at low-medium temperature (425-650°C) in order to promote stress relaxation and transform any supersaturated β and/or brittle α′ (martensite) to the α-phase [21, 37, 44]. Bi-modal microstructures are often selected for use in fan and compressor blades due to their high cycle and low cycle fatigue resistance whereas β-annealed microstructures are more suited to structural components [36]. Optical micrographs of typical martensitic, bi-modal and β-annealed microstructures are provided in Fig. 2, with the characteristic processing routes outlined in Fig. 3 [36].

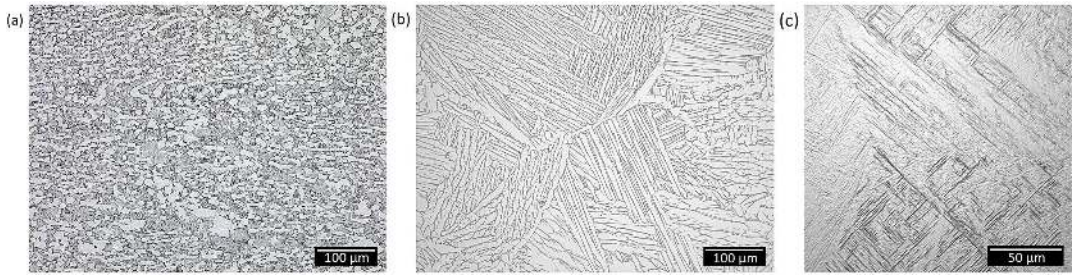

Figure 2: Optical micrographs characteristic of β-annealed (a), bi-modal (b), and martensitic (c) microstructures. Note: β-phase is shaded in grey, with α-phase shaded in white.

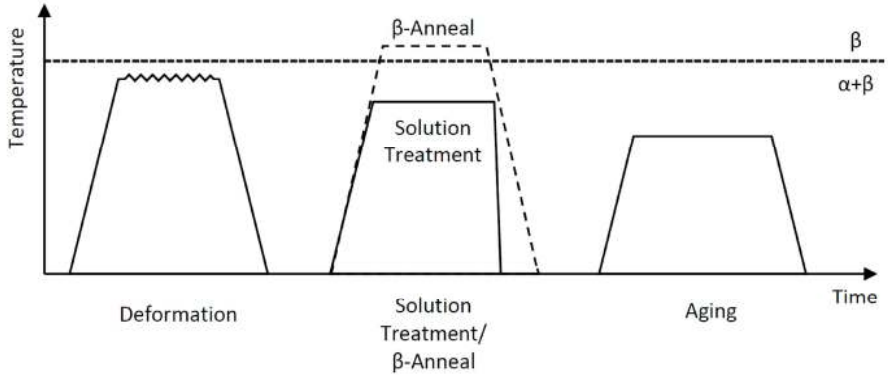

Figure 3: Typical processing route for β-annealed (dashed line) and bimodal (solid line) microstructures [36].

Alternatively, stress relief annealing above 550°C can be carried out directly after deformation to produce the so-called mill annealed microstructure. This is a very common condition yet the process parameters are ill defined [36]. Mill-annealed microstructures

are often used for large forgings but the more expensive β-annealed microstructure provides better resistance to fatigue crack propagation so is used for critical parts such as bulkheads [36].

Post weld heat treatment is an annealing treatment commonly employed to reduce localised residual stress distributions formed due to extreme temperature gradients during welding. This typically involves heating to a medium temperature (~650°C), holding for 1-2 hours, followed by an air cool [45]. The decreased thermal gradients inherent to air cooling tend to have minimal adverse effect on residual stress. Similar heat treatments have been utilised for additively manufactured Ti-6Al-4V, with further treatments at increased temperatures to induce favourable microstructural changes [46, 47, 48, 49].

Thus, heat treatment is used to produce microstructures with tailored mechanical properties, yet adverse residual stresses may be formed inadvertently. Annealing stages are commonly employed to reduce the magnitude of such stresses but quantitative prediction is not yet readily available [50].

2. Thermo-Metallo-Mechanical Modelling of Residual Stress

In order to develop a predictive model for thermo-mechanically induced residual stress evolution, one must consider three interrelated physical fields, or sub-models, which incorporate thermal analysis, metallurgical transformation and mechanical response [50]. These sub-models are interrelated by couplings which can have a significant effect on each other and are underpinned by the underlying material properties. Additional interactions and sub-models such as fluid dynamics and electromagnetic influences have been discussed by Gür and Şimşir [51] but are not deemed essential for thermo-metallo-mechanical (TMM) modelling of residual stress due to heat treatment [44].

The majority of previous modelling studies follow a similar procedure that includes (i) identification of problem, (ii) collection of input data and development of

physical principles, (iii) process modelling; mainly using finite-element analysis (FEA), and (iv) validation by experimental measurements. However, a number of differences lie in the model assumptions, input data collected, and the measurement methodology used for experimental validation [50, 52].

Thermal gradients in a workpiece induce unequal thermal expansion and contraction, producing a thermal strain component, and phase transformation. Phase transformations can lead to changes in unit cell volume and transformation induced plasticity which contributes to generation of strain gradients [53]. Additionally, a mechanical strain component exists as a result of the thermo-mechanical material history [44, 53]. These strain components have a summative effect on the total strain; and therefore residual stress. This total strain, ε_{ij}^{total}, can be expressed using infinitesimal strain theory as [54]:

$$d\varepsilon_{ij}^{total} = d\varepsilon_{ij}^{mech} + d\varepsilon_{ij}^{met} + d\varepsilon_{ij}^{th}$$

Where ε_{ij}^{mech} is the mechanically induced component of strain, ε_{ij}^{met} is the metallurgically induced component of strain, and ε_{ij}^{th} is the thermally induced component of strain.

However, metallurgical changes may also lead to variations in thermo-physical properties, such as latent heat, which affects the temperature field; consequently affecting thermal strain and phase transformation [51]. Similarly, increased total strain may lead to stress induced transformations [55], and mechanical deformation can generate heat [51].

The complexity of a fully coupled model which incorporates all sub-models and their relationships, has led to the vast majority of previous studies electing for a sequential model with simplifying assumptions [11, 13, 15, 56]. Some couplings can be neglected regardless of thermo-mechanical process conditions, whereas others are dependent on the process conditions and the specific material. For example, heat generation due to

mechanical work is insignificant during heat treatment and therefore its effect on thermal analysis can be neglected [13]. Similarly, the influence of latent heat on temperature distribution has historically been deemed insignificant and ignored for the majority of solid-state transformations [57], yet a recent study concerning additive manufactured Ti-6Al-4V has observed an inflection of cooling curves at approximately 800°C which may be attributed to latent heat, warranting further investigation [58]. On the other hand, depending on the heat treatment temperature and cooling rate, phase transformations can induce significant strains; and *vice-versa* [50]. Such metallurgical couplings may be initially assessed based on the time-temperature-transformation (TTT) or isothermal transformation (IT) diagram. The relationship between the three sub-models for heat treatment of Ti-6Al-4V is presented in Fig. 4; with dashed arrows representing the couplings which can be neglected. The critical outputs of such models are commonly: residual stress, distortion and final microstructure. Thus, based on the aforementioned simplifications one may consider the overall model in order of (i) thermal, (ii) metallurgical and (iii) mechanical sub-models, which are explained in detail in the following sections [50, 51, 59, 60, 61].

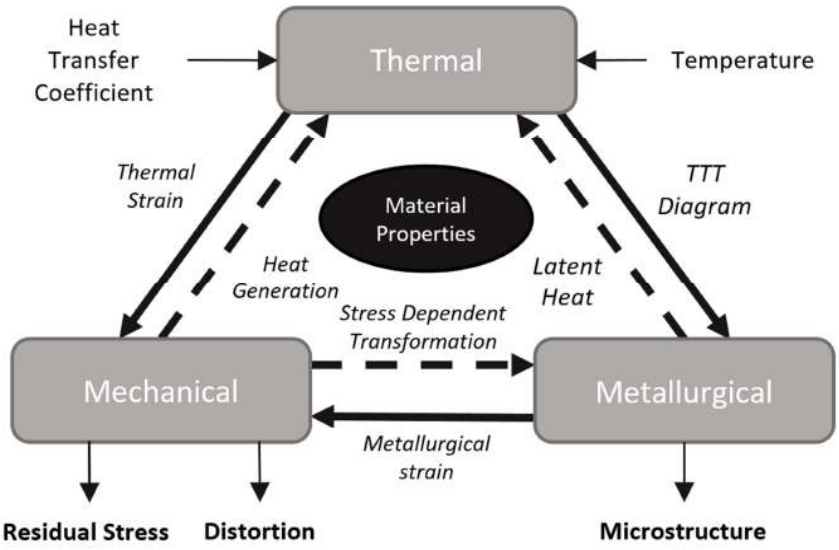

Figure 4: Physical sub-models and couplings for simulation of thermo-mechanical processing of metals. Strong couplings signified by solid lines, weak couplings signified by dashed lines. Adapted from [50, 51, 59, 60, 61].

Thermal Sub-Model

For static heat treatment, conductive heat transfer is assumed within the part, and heat loss can be approximated assuming convective, radiative or conductive heat transfer depending on the fixture conditions and cooling conditions [44].

The inputs of the thermal sub-model, out-with material properties, are initial temperature and heat transfer coefficient (HTC). The heat transfer coefficient governs the cooling rate throughout a part and is a function of both temperature and location in the part, making it difficult to estimate or find reliable pre-existing data. To that end, initial experiments are often conducted to provide accurate heat transfer coefficient data [14, 62, 63, 64].

The inverse HTC method can be used to determine accurate HTC's for various cooling conditions, as shown by Dye *et al.* [14], where the procedure was carried out to ascertain the effect of different quenching media; water, air and oil, on the HTC and evolution of residual stress in IN718. As expected, both experimental and simulated data found that air cooling led to lower heat transfer and hence residual stress throughout the part compared with oil and water quenching. Majorek *et al.* [62, 63] displayed the importance of location dependent HTCs for residual stress simulation of water quenched components. Thus, experimental HTC data pertaining to the sample geometry of interest is highly important to ensure accurate residual stress prediction.

The thermal component of strain is caused by non-uniform thermal gradients in the part which lead to differential thermal expansion or contraction of the material. Therefore, thermal strain can be calculated using the coefficients of thermal expansion alongside knowledge of the thermal field. Bhatti *et al.* [65] found that temperature dependant thermal expansion coefficients are vital for accurate prediction of welding

induced residual stress. This has been reinforced by additional sensitivity analyses [66, 67].

Temperature dependent thermal expansion coefficients are typically experimentally obtained using dilatometry which measures the macroscopic expansion due to temperature change [68]. However, this macroscopic thermal expansion is composed of thermal lattice induced strain as well as a transformation induced volume change strain component, ε_{ij}^{tv}; which are dependent on phase transformation [68] . Some take this into account by assuming that ε_{ij}^{tv} is independent of initial microstructure and can therefore be considered as a component of ε_{ij}^{th} within the thermal sub-model rather than the metallurgical sub-model [19, 20, 69]. Other studies have used data gathered by X-ray diffraction (XRD), whereby thermally induced lattice expansion of individual α and β phases were measured, allowing for the lattice expansion due to thermal fluctuations to be separated from transformation induced volume changes [33, 70]. Careful consideration must be taken when using literature values for thermal expansion to ensure that one does not consider both macroscopic expansion as well as separate lattice expansion which may effectively consider lattice expansion twofold [5]. Both methodologies have advantages and disadvantages. Thermal expansion coefficients gathered by dilatometry are more commonly available and lead to increased simplicity by eliminating the need to include a separate ε_{ij}^{tv} component in the overall TMM model. On the other hand, if the model is likely to be used for a range of process conditions and initial microstructures; which will invariably lead to differences in transformation rates and therefore transformation induced volume changes, this would affect the value of apparent thermal expansion, and therefore the lattice parameter based method may be more appropriate under these circumstances. However, a quantitative comparison of how these methodologies affect residual stress prediction has not yet been studied for Ti-6Al-

4V. Thermal lattice expansion can be taken for each phase, forming the thermal strain component, ε_{ij}^{th} [70]:

$$\varepsilon_{ij}^{th} = \Delta T \sum_{i=1}^{n} \alpha_i (T_0) f_i (T_0 + \Delta T)$$

Where T_0 is the initial temperature, ΔT is the change in temperature, α_i is the lattice expansion of phase *i*, and f_i is the volume fraction of phase *i*; for *n* number of phases.

If one calculated thermal expansion based solely on lattice expansion data (Fig. 5 [33]), transformation induced volume strain, ε_{ij}^{tv}, can also be calculated, but as this is a metallurgical mechanism, it is more suitably placed as a component of the metallurgical strain, ε_{ij}^{met} , and will be discussed in the subsequent section.

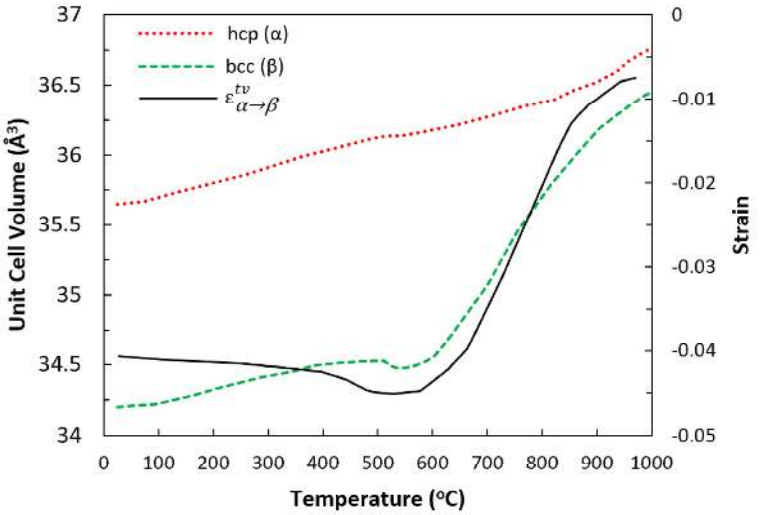

Figure 5: Temperature dependent variation of α and β phase unit cell volumes and accompanying transformation induced volume change strain, obtained by synchrotron X-Ray diffraction. (Adapted from [33]).

The majority of thermo-physical material properties, excluding mechanical properties, tend to be assigned once the thermal field is known [67]. This is partially based on the assumption that these properties do not vary significantly between differing microstructures and also due to the difficulties associated with gathering phase specific thermo-physical properties in dual phase materials, and lack thereof experimental data [17, 51]. Sensitivity analyses have found that thermal conductivity, heat capacity and

density have a minimal effect on predictive outputs, providing that temperature dependence is taken into account, and are presented alongside the macroscopic based thermal expansion coefficient in Fig. 6 [65, 66, 67, 71, 72]. It should be noted that bulk thermal conductivity may vary dependent on the quantity of alloying elements within the parent titanium matrix. Electrical resistivity was measured for a number of titanium alloys with varying compositions of aluminium and vanadium similar to the limits possible in Ti-6Al-4V, over a range of temperature [73]. This can be related to thermal conductivity using the relation developed by Powell and Tye [74], showing less than 10% deviation between alloys. This is unlikely to significantly affect residual stress prediction based on the sensitivity analysis of Zhou and Chao [67].

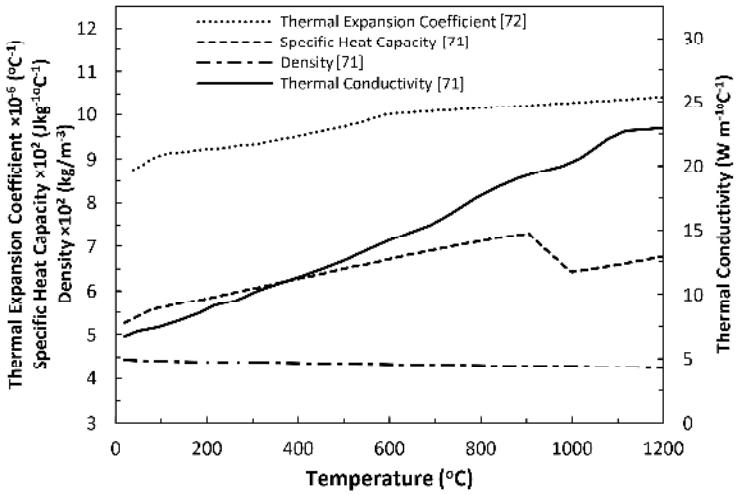

Figure 6: Selection of temperature dependant physical properties used in thermo-metallo-mechanical modelling of Ti-6Al-4V [71, 72].

Metallurgical Sub-Model

The metallurgical sub-model can be used to not only predict the metallurgically induced components of total strain, but also evolution of microstructure. As the focus of this review was residual stress prediction, microstructure prediction is not discussed in detail, however the reader is directed to the following works concerning microstructure modelling for further information [75, 76, 77, 78]. The metallurgical component of strain, ε_{ij}^{met}, is said to be composed of [54]:

$$\varepsilon_{ij}^{met} = \varepsilon_{ij}^{tv} + \varepsilon_{ij}^{tp}$$

Where ε_{ij}^{tv} is the transformation induced volume change component of strain, and ε_{ij}^{tp} is the transformation induced plasticity component of strain. Such strains are dependent on the phase transformations which occur within the material. These can be differentiated by the underlying mechanisms; diffusion controlled, or martensitic transformations. A schematic describing the major transformations in Ti-6Al-4V are provided in Fig. 7 [76].

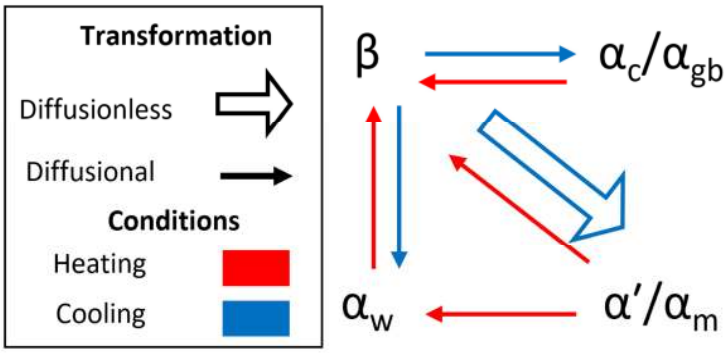

Figure 7: Schematic diagram showing nature and conditions for formation of major phases and morphologies in Ti-6Al-4V alloy. (Adapted from [76]*).*

The diffusion controlled β↔α+β transformation in Ti-6Al-4V has been approximated using Johnson-Mehl-Avrami-Kolmogorov (JMAK) based kinetics, with a number of experimentally determined transformation curves to support this (see Fig. 8) [32, 79, 80]. However, experimental techniques such as resistivity, synchrotron XRD and differential scanning calorimetry (DSC) do not allow for simple discrimination of α morphology. This has been addressed by JMatPro thermodynamic-based software; which uses separate JMAK parameters for each of two distinct morphologies; colony α (α_C)/grain boundary α (α_{GB}) and Widmenstätten α (α_W) [81]. Kelly incorporated this into a thermo-metallurgical model for metal deposition of Ti-6Al-4V, showing qualitative accordance with microstructural and morphological observations [76]. This model was further developed by Charles, incorporating α lath width prediction, which can be related to properties such as yield strength; and has been termed the Kelly-Charles model [78, 82, 83]. A selection of TTT curves describing the β→α+β transformation and

morphologies are presented in Fig. 8 [27, 76, 79, 80, 83, 84, 85, 86]. Such transformation is usually characteristic of medium-low cooling rates below 20°C/s, typical of air and furnace cooling [27, 43]. This is reiterated by the findings of Ahmed and Rack [43] who observed β→α+β transformed microstructures for cooling rates of 1.5-20°C/s. These curves also compare reasonably well with the experimental based curves of Sieniawski *et al.* [27] in terms of the onset of transformation at high temperature, however discrepancies arise below 700°C.

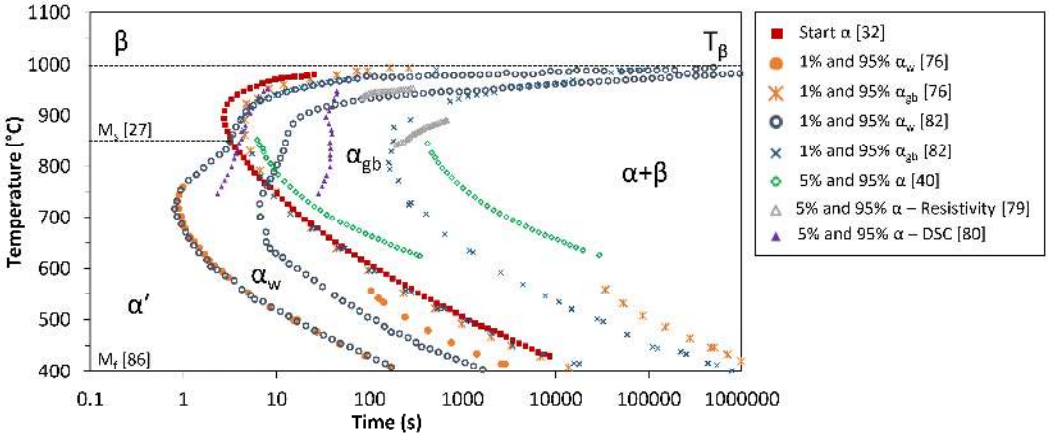

Figure 8: Time-Temperature-Transformation Diagram for Ti-6Al-4V with comparison of selected transformation curves used in previous studies. [27, 76, 79, 80, 83, 84, 85, 86]

On the other hand, the diffusionless martensitic transformation which occurs during the β→α′ transition is typically described by a Koistinen-Marburger (KM) type equation [87]. This is more often associated with high cooling rates, observed during water quenching operations. A separate morphology, termed massive α (α_m) has been observed between cooling rates typical of the β→α+β and β→α′ transformation [43]. This is also typically described by a KM-based equation [70]. The displacive nature of the martensitic transformation can lead to transformation induced plasticity (TRIP) [88]. This is created as a result of type II strains produced by transformation induced volume changes which interact with external and type I residual stress to generate a plastic strain upon completion of phase transformation [55]. It is further defined as significantly increased plasticity during phase transformation, which may allow for the

accommodation of thermal strains without accumulation of elastic strain and has been studied extensively in steels, yet there are few investigations regarding titanium alloys [89, 90]. Transformation induced plasticity is typically described by two mechanisms, the Greenwood-Johnson mechanism and the Magee mechanism [91, 92]. The transformation induced plasticity component of strain is primarily due to the Greenwood-Johnson mechanism and is described by [51]:

$$\varepsilon_{ij}^{tp} = K_{ij}^{tp} \Delta f_m s_{ij}$$

Where K_{ij}^{tp} is a material specific constant, Δf_m is the change in martensite volume fraction and s_{ij} is the deviatoric component of stress. A number of expressions exist for K_{ij}^{tp}, as discussed by Dalgic and Lowisch [93], with the following used by Teixeira *et al.* [53] for Ti17:

$$K_{ij}^{tp} = \frac{5}{6}\frac{1}{\sigma_e}\frac{\Delta V}{V_0}$$

Where σ_e is the yield strength of the weaker phase, β; ΔV is the change in unit cell volume and V_0 is the original unit cell volume. These equations were formulated based on experimental data for steels and may therefore lead to inaccuracies when applied to titanium alloys due to the presence of the hcp crystal structure [50, 88]. It is therefore recommended that further fundamental studies are conducted to understand the transformation induced plasticity behaviour in Ti-6Al-4V. Additionally, the martensitic transformation in Ti-6Al-4V is often a point of contention between authors insofar as the onset temperature of the martensitic transformation varies drastically throughout the literature. An M_s of 575°C was used in the work of Ahmed and Rack [43], whereas Crespo *et al.* [94] assumed 650°C, and 850°C was stated by Sieniawski *et al.* [27], based on experimental observations. Elmer *et al.* [85] observed an apparent M_s below 600°C when carrying out in-situ time resolved XRD. Such differences are significant and whilst this

may be partially due to differences in local phase chemistry, predominantly α- and β-stabiliser composition, it could also be due to additional kinetic factors which are not yet fully understood. Although sensitivity analyses have been performed by both Charles [83] and Ahn [54], showing that variation in M_s has little effect on the computed martensite fraction in microstructure models, such discrepancies may have a profound effect on the development of residual stress. For example, if the assumed martensitic start temperature was lower than the true M_s, associated transformation induced plasticity strains would lead to false prediction of accommodation of thermal strains accumulated upon cooling. Thus, leading to under-prediction of the final residual stress state.

Following the elucidation of phase transformations, the aforementioned transformation induced volume change strain, ε_{ij}^{tv}, can be calculated based on the difference in unit cell volume associated with the phase transformation:

$$\varepsilon_{i\to j}^{tv} = \frac{\Delta \mathrm{V}}{V_0}$$

Where $\varepsilon_{i\to j}^{tv}$ is the transformation specific volume change strain, $\Delta \mathrm{V}$ is the change in unit cell volume and V_0 is the original unit cell volume. The total transformation induced volume change strain can then be computed for *n* phases:

$$\varepsilon_{ij}^{tv} = \sum_{i=1}^{n} \varepsilon_{i\to j}^{tv}\, \Delta f_i$$

Fig. 5 shows the variation of $\varepsilon_{\alpha\to\beta}^{tv}$ below the β-transus temperature, experimentally obtained by Elmer *et al*. [33] using synchrotron XRD. Local composition has also been found to influence unit cell dimensions, which may introduce type II stress [95]. However, the macroscopic thermal expansion is often used rather than that based on lattice parameters in TMM modelling (see Table 4), effectively making a separate expression for ε_{ij}^{tv} redundant.

Mechanical Sub-Model

The constitutive behaviour of α+β titanium alloys is complex during heat treatment. Mechanical properties are dependent on temperature, microstructure, deformation and strain rate to varying degrees and are therefore sensitive to the thermal and metallurgical sub-models [96, 97]. Traditionally, experimental data has been used with linear interpolation between temperatures, however this is cost intensive and the relationship is not always directly proportional, leading to the preference for mathematical models to describe the behaviour.

A number of constitutive models have been developed to calculate the strain associated with elastic (ε_e), visco-plastic (ε_{vp}), and creep (ε_{cr}) phenomena in Ti-6Al-4V alloy. The summative total of these strain components can be taken as the mechanical contribution towards strain (ε_{mech}) [70]:

$$d\varepsilon_{ij}^{mech} = \ d\varepsilon_{ij}^{e} + d\varepsilon_{ij}^{vp} + d\varepsilon_{ij}^{cr}$$

The elastic component of strain is commonly calculated according to Hooke's Law, however visco-plastic and creep behaviour have been described by a number of different models [98]. Constitutive models are often based on one of two principles including empirical models, and physically based models. Empirical models are synthesised by fitting equations to experimental data with little consideration for the underlying physical processes which cause the mechanical behaviour, whereas physically based models attempt to address the underlying physical mechanisms. The benefits of empirical models include ease of implementation due to the relative simplicity and requirement of fewer input parameters, however such models have limited predictive power and are therefore not recommended for use outside the range of process conditions and initial microstructures to which they were originally calibrated. On the other hand, despite their complexity, physically based models take a more comprehensive range of underlying

phenomena into account, leading to improved ranges of validity in addition to the opportunity to integrate metallurgical parameters within the model.

A number of authors have assumed that plastic strain is independent of strain rate at a given temperature [19, 70, 99]. However this is not the case for Ti-6Al-4V; which has high strain rate sensitivity at low strain rates and elevated temperatures [100]. A quantitative comparison of independent and strain rate dependent flow stress by Navalho *et al.* [13] showed that the assumption of the former has a strong influence on the predicted magnitude of residual stress. Therefore, the deformation behaviour should be considered visco-plastic, or strain rate dependent when modelling heat treatment.

The Johnson-Cook (JC) model is one of the most widely used empirically based flow stress prediction models [101, 102, 103]. The model has been found to provide reasonable agreement with experimental data for Ti-6Al-4V over a range of temperatures, at both low and high strain rates, as shown by [104] and [105], respectively. However, the multiplicative nature of the relation has been said to limit the range over which it is applicable which is undesirable when considering heat treatment applications [106]. This can be shown for the JC model employed by Seo *et al.* [107] (see Fig. 9) as it appears to lose validity above 600°C. Other empirical relations have been applied to Ti-6Al-4V including the Fields-Backhofen and Khan-Huang-Liang models but physically based models were preferred as they tend to consider microstructure dynamics more accurately [104, 108].

Semiatin *et al*. [109] developed a semi-empirical model which considered a summative yield stress based on separately calculated α and β phase components for an equiaxed starting microstructure. The model provided some insight into strain partitioning in Ti-6Al-4V which has been further investigated. The constitutive model has been applied by Crespo *et al.* [94] for the modelling of residual stress. However, the

original model was calibrated for use in forging simulations over the range of 815-1000°C and loses accuracy outside these bounds; this is particularly exemplified in Fig. 9.

A number of physically based models have been developed [98, 106, 110, 111, 112] based on the work of Conrad [113] who stated that the dominant deformation mechanism of plastic flow in titanium is dislocation movement by glide and climb, which is aided by diffusion. At low temperatures, plastic flow is determined by the concentration of interstitial solutes, whereas at high temperatures the concentration of interstitial impurities has a more significant effect. The flow stress can therefore be expressed using the Mecking-Kocks formalism [114] as so-called athermal and thermally activated stress components, respectfully:

$$\sigma = \sigma_{\mu}(\mu, \varepsilon, D, C_s) + \sigma^*(T, \dot{\varepsilon}, C_i)$$

This model was first applied to Ti-6Al-4V by Follansbee and Gray [115], and has been further developed by others. The Picu-Majorell [106] model addressed a lack of previous constitutive models which took the heterogeneity of α and β-phases into account. The model was calibrated using compression data over a range of strain rates (10^{-3} s^{-1} to 10 s^{-1}) and temperatures (-196-1127°C) [106]. However, as this work focussed on applications for forging of equiaxed initial microstructures where globularization is not a major mechanism, such a model may have limited applicability to heat treatment of lamellar and bimodal microstructures; where globularization can have a major effect at temperatures of 800-975°C and strain rates below 10^{-2} s^{-1} which is typical of heat treatment conditions [116]. This was addressed by Babu for a bimodal initial microstructure, and by Gao for a lamellar microstructure; yet with added complexity [117]. The Babu model has also been coupled with the metallurgical model developed by Charles which accounts for non-isothermal phase transformation [69]. These models were calibrated over a similar range of temperatures and strain rates to that of Picu and Majorell

[106, 118]. The Picu-Majorell model compares well with experimental data from numerous sources, considering strain rates as low as 10^{-4} s^{-1}, in the temperature range of 20-1000°C. This model is shown to accurately predict flow stress over this range of temperatures in Fig. 9, with good agreement with experimental data as well as the JC and Semiatin models below and above 600°C, respectively [106, 107, 109, 115, 118, 119, 120, 121, 122]. This highlights the ability of such physically based models to predict over a wide range of temperatures where opposing mechanisms dominate [123]. However, based on the findings of Semiatin *et al.* [109], these models do not adequately take strain partitioning into account, yet this aspect has been accounted for in a similar model [112]. Strain partitioning is of particular importance during high temperature deformation within the α+β phase field as elastic strain is disproportionally accommodated within the harder α phase whilst the β phase is more susceptible to plastic deformation, leading to the introduction of type II residual stress on release of external load [124]. An additional physically based model has been developed by Alabort *et al.* [100] for flow stress in the superplastic region; 850-950°C and 10^{-3}-10^{-5} s^{-1}, however the accuracy of this model at temperatures below 700°C is not known.

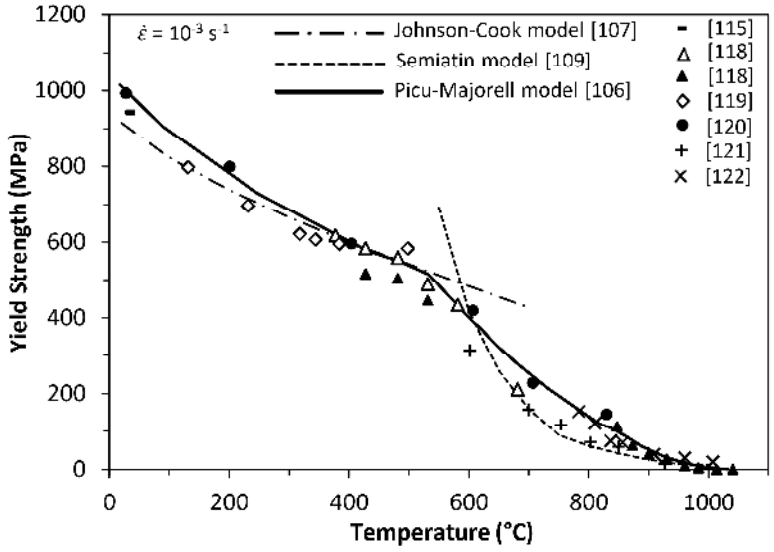

Figure 9: Comparison of temperature dependent 0.2% yield strength computed using Johnson-Cook, Semiatin and Picu-Majorell models against experimental data for a constant strain rate of 10^{-3} s^{-1} in the region of 20-1030℃. [106, 107, 109, 115, 118, 119, 120, 121, 122]

Comparatively fewer works have attempted to develop models describing the creep strain component, which is often based on observed stress relaxation behaviour alongside the deformation mechanism maps such as that presented by Prasad and Sasidhara [98, 125, 126]. A number of previous studies have assumed that the creep strain component is negligible [70] or have applied simplified stress relaxation models [99]. This was applied to additive manufacturing and welding cases but is unlikely to adequately account for the phenomena during heat treatment, which is generally over a longer timescale, as this been seen to have a significant effect on residual stress relaxation above temperatures of 477°C [40]. Babu *et al.* [110] adapted their plasticity model to predict stress relaxation behaviour, which was able to compute stress decay, albeit at a much slower rate than that exhibited by experimental data. Kim *et al.* [127] produced a physically based stress relaxation model established on the internal variable theory of inelastic deformation and experimental observations. Grain matrix deformation (i.e. dislocation glide and climb) and grain boundary sliding relaxation mechanisms were considered. It was noted that grain matrix deformation was the dominant high-temperature (720-900°C) mechanism for α lath widths ranging from 1-8 μm. This was the case for low levels of pre-strain (ε=0.05), however grain boundary sliding was found to be operating for heavily pre-deformed (ε=1.2) samples, particularly 1 μm lath width, at temperatures of 815-900°C [127]. This is supported by additional observations of the emergence of grain boundary sliding as a dominant mechanism at elevated temperatures (>750°C) for creep rates below 10^{-3} s^{-1} in equiaxed and bimodal microstructures [126, 128]. However, Wang *et al.* [47] found that grain matrix deformation was dominant in the region of 600-700°C for both equiaxed and Widmenstätten starting microstructures. More recently, the effect of microstructural differences on stress relaxation response was further exemplified for differing α grain sizes in equiaxed microstructures between 700-900°C [129]. Yan *et al.*

[130] noted that previous experimental data [125, 126] followed a power law based trend and produced a simplified Arrhenius model for an equiaxed starting microstructure which was validated from 550-700°C. However, this power law based model does not take grain boundary sliding into account and a mechanistic model, as used by Kim *et al.* [127, 128, 131], may be more accurate at elevated temperatures. Even so, when one compares the stress relaxation data obtained by Lee *et al.* [129] to that of Alabort *et al.* [132] (Fig 10), for similar initial microstructures, good agreement is found at 600°C, however there is a significant deviation in response above this temperature. The reason for this deviation is unclear and merits further investigation into stress relaxation behaviour of Ti-6Al-4V.

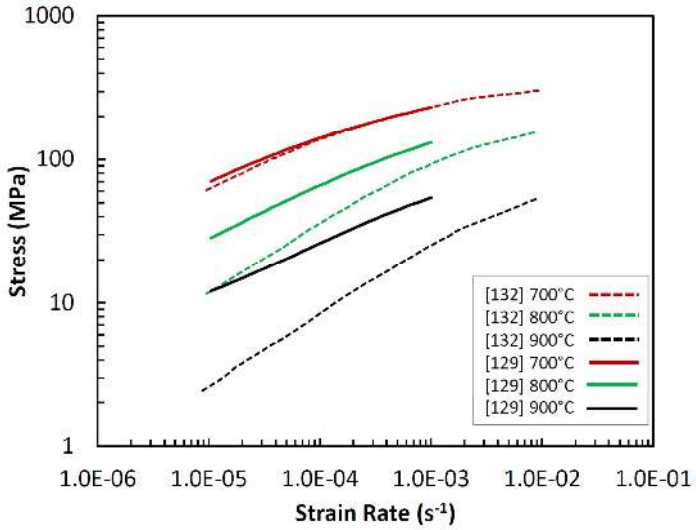

Figure 10: Comparison of experimental stress relaxation response obtained by Alabort et al. [132] and Lee et al. [129] for Ti-6Al-4V under load relaxation conditions.

The apparent strong dependence of initial microstructure on stress relaxation response in Ti-6Al-4V, and the various achievable microstructural variants, suggests that sufficient material specific experimental data must be gathered prior to the adoption or development of an accurate constitutive relation for creep strain.

Model Validation

It is imperative to validate computer simulated TMM models against experimental data to ensure model accuracy and inform future research [52, 133, 134]. This can be done by

comparing the output parameters of residual stress, microstructure or distortion (Fig. 4) for a material that has been exposed to controlled thermal cycling against that which has been measured experimentally.

Microstructure and distortion analysis is relatively straightforward but each residual stress measurement technique has specific attributes which must be considered for each application. For example, compressive surface and near surface residual stress can reduce fatigue crack propagation rate, whereas bulk residual stresses have a significant effect on overall structural integrity [135]. A non-exhaustive summary of selected measurement techniques is presented in Table 3. Detailed discussion of the numerous available techniques can be found elsewhere [7, 136, 137, 138, 139, 140, 141, 142]. Of particular note are the reviews presented by Withers and Bhadeshia [6, 7], and that of Rossini *et al.*[138] which presents a visual summary of penetration depth and spatial resolution for nine residual stress measurement techniques. The most popular validation techniques used are XRD and hole drilling. These techniques were among the first developed and constituted over 50% of residual stress measurements in 2001 [137]. This is evident in their application for validation in early predictive studies [7, 143].

Table 3: Comparison of selected residual stress measurement techniques.

Method	Material Removal	Penetration Depth in Ti-Alloys	Spatial Resolution	Accuracy	Comments
X-Ray Diffraction	Non-destructive	< 50 µm [7]	1 mm laterally [7]	±20 MPa [7]	Biaxial surface stress point measurements
Hole Drilling	Semi-destructive	1.2 × hole diameter [7]	5 µm depth (ESPI) [144]	±50 MPa [7]	Biaxial stress (at depth increments)
Contour Method (Conventional)	Destructive	Through sample thickness [145]	Dependent on measurement resolution, knot spacing and element size [145]	Larger of ±17 MPa or ±10% of measured stress [145]	Uniaxial 2-D out-of-plane stress plot
Neutron Diffraction	Non-destructive	< 10 mm [i] [146]	0.5 mm [ii] [147]	50 µε [ii] [147]	Triaxial stress point measurements

i Chalk River Laboratories, Canada
ii Engin-X, ISIS Neutron and Muon Source, UK

XRD has been used by Zhang *et al.* [148] to verify the simulated residual stress distribution in quenched aluminium alloy 2024 forgings. The axial and longitudinal surface residual stress components were recorded at three positions for each quench condition, showing good accordance with the simulated for most points. Diffraction-based measurements are more difficult in titanium alloys which can exhibit weak peak intensities and broadening due to the influence of texture [149], yet successful measurements have been reported for Ti-6Al-4V [150, 151, 152].Additionally, diffraction elastic constants (DEC) must be known when using diffraction based techniques, such as XRD and neutron diffraction. Whilst the DEC of pure titanium can be used [153], it is dependent on process history and the use of Ti-6Al-4V specific data is deemed more robust [154]. However, as XRD has limited penetration depths, this restricts the extent to which the model can be validated. Therefore, XRD is commonly combined with layer removal to provide near-surface as well as surface residual stress, though this can be time consuming and alter the residual stress distribution at points of interest [143, 148, 155].

Tanner and Robinson [12] modelled residual stress evolution due to water quenching in rectilinear 7010 aluminium forgings of various dimensions using ABAQUS FEA software. Two complimentary residual stress measurement techniques were utilised: strain gauge rosette based hole drilling stress measurement at a depth of 2 mm from the surface, and XRD for surface stress measurement. Reasonable agreement was found between predicted and measured residual stresses using hole drilling, however the model under-predicted all surface stresses when compared with XRD. This under-prediction was attributed to a lack of plasticity information in the model database, recommending further thermo-mechanical characterisation. The combination of two complimentary surface and near-surface residual stress measurement techniques proved useful for model verification and analysis. However, upon considering the maximum measurement depth of 2 mm against the maximum forging dimensions of 124×156×550 mm, further verification by through-thickness residual stress measurement may have been beneficial. A technique related to conventional hole drilling, deep hole drilling, may be used to provide through-thickness data [142, 156]. However, Hosseinzadeh *et al.* [157] compared the residual stress results from deep hole drilling with simulated data and found large discrepancies which were attributed to stress relaxation due to deep hole drilling rather than issues with the model itself. However, reconstruction of deep hole drilling results, accounting for plasticity, using FEA has shown better agreement with model predictions [157, 158]. A further limitation of hole drilling techniques is that only a 1-D depth profile is attained, albeit for two stress components [7].

Dye *et al.* [14] utilised neutron diffraction to validate residual stress prediction in air, oil and water quenched IN718 cylinders of 20 mm diameter. This allowed for non-destructive measurement of triaxial residual stress from a depth of 0.5 mm to the centre of the part, which can be approximated as through-thickness measurement if axisymmetry

is assumed. Seven measurements were taken in each direction for all three quenchants. There was good agreement between predicted and measured residual stresses for the cylinders, particularly water and oil quenched conditions. However, neutron diffraction has limited resolution in the near-surface region which is likely to have significant residual stress gradients in quenched materials [146]. Thus, use of a complimentary near-surface technique may prove beneficial. A similar study was later conducted by Rist *et al.* [159], yet this again lacked model validation through near-surface measurements. Additionally, an economical penetration depth is usually stipulated; approximately 10 mm for titanium [146], which limits the effective depth to which the technique can be applied.

The contour method was employed by Navalho *et al.* [13] to validate the simulation of residual stresses due to quenching in forged rectilinear aluminium blocks. Three blocks were subjected to identical heat treatment conditions followed by EDM cutting along symmetry planes in three directions, followed by contour method analysis, producing a triaxial representation of stress. The results were then compared with the respective 2D representation of out-of-plane stress at these locations as determined by the finite element model. Good agreement was found between contour method and simulated results, with a maximum deviation of 25% throughout the parts. Regions of peak tensile and compressive stresses also showed good accordance. Poorer agreement was noted around the sample edges and this was attributed to the reduced accuracy of the contour method in this region. However, no additional validation was conducted near the sample surface where higher thermal – and in turn residual stress – gradients are more likely to lead to increased deviation from model predictions, as discussed by Tanner *et al.* [10]. Furthermore, the use of sacrificial material has been found to improve near-surface accuracy of the contour method, especially for quench operations where high magnitudes

of near-surface residual stress is common [64, 145]. Bühr *et al.* [18] and Hönnige *et al.* [49] used a combination of the contour method and neutron diffraction on Ti-6Al-4V, showing good agreement between techniques. Although the conventional contour method provides a 2-D map of out-of-plane stress, this is limited to uniaxial stress unless additional contour cuts; the multiple cut contour method, or alternative measurements; the surface superposition contour method, are taken [160, 161]. Additionally, when compared with other measurement techniques such as hole drilling or XRD, the contour method is relatively young, with limited understanding of the accuracy and errors associated with the technique [145].

Based on the aforementioned studies, it is clear that there is no universal residual stress measurement method which can provide accurate measurements of surface, near surface and through-thickness stress distributions. In order to overcome the limitations of using a single measurement technique, one may employ two or more complimentary techniques. Tsivoulas *et al.* [162] used a combination of XRD and neutron diffraction to characterise both surface and through-thickness residual stress in flow formed steel tubes. Both techniques are non-destructive, but limited near-surface resolution would be attainable [162]. Similar near-surface resolution issues persist when considering the combined contour method and XRD methodology used by Xie *et al.* [45] for welded 10 mm thickness Ti-6Al-4V where the contour data within 0.4 mm of the edges was not considered for data processing. Such limitations of the contour method were minimised by Pagliaro *et al.* [160, 161] who developed a methodology for accurate near-surface data, however it was recommended that additional techniques such as incremental hole drilling or XRD with layer removal may be used for increased confidence of near-surface data. This was addressed by Conroy *et al.* [163] who employed neutron diffraction, the contour method, incremental hole drilling and XRD, showing much improved near-surface

measurement sensitivity of the hole drilling method when compared with the contour method.

A similar methodology was also utilised by Rae *et al.* [150] who used a combination of XRD, electronic speckle pattern interferometry (ESPI) based incremental hole drilling and the contour method to provide the surface, near-surface and through-thickness residual stress distribution in electron beam welded Ti-6Al-4V rings. Good agreement was found between the hole drilling and contour data at various depths; and XRD measurements verified the expected trend in surface residual stress distribution. This is illustrated in Fig. 11 [150]. The 2-D residual stress maps obtained by the contour method were correlated to microhardness and microstructural observations. The complimentary measurements afforded by employing multiple techniques including XRD, hole drilling and the contour method have been further exemplified [142, 151].

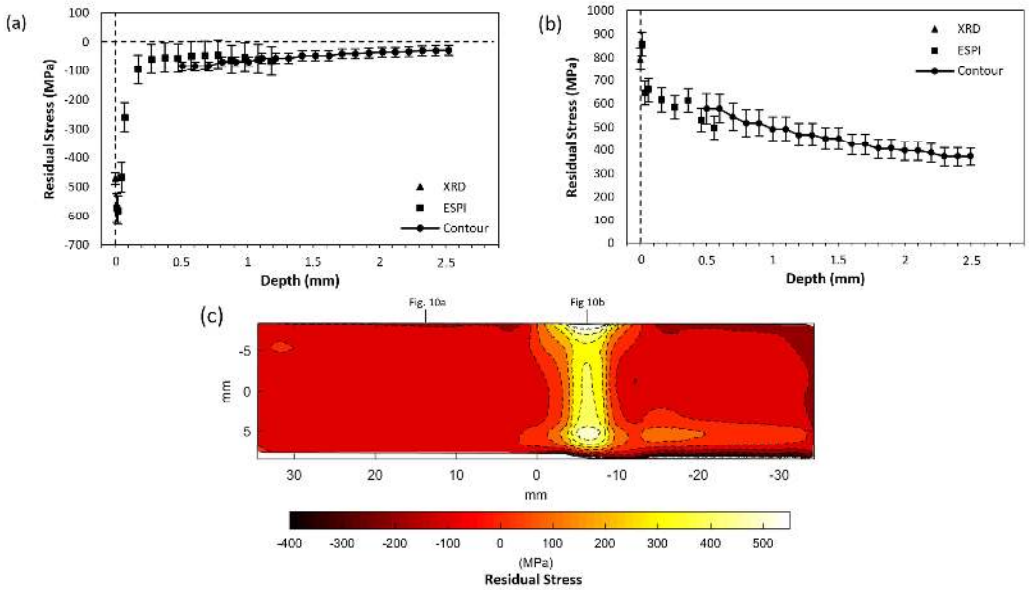

Figure 11: Example application of multiple complimentary techniques for residual stress measurement in electron beam welded Ti-6Al-4V. Line profile comparing XRD, ESPI based hole drilling and the contour method in: (a) the bulk material; and (b) the fusion zone. A 2-D map of out-of-plane residual stress is presented in (c) with line profile points highlighted. (Adapted from [150]).

Thus, a number of approaches may be employed for validation of residual stress prediction models, yet the use of multiple complementary measurement techniques may provide a more robust comparison.

3. Discussion

A summary of recent investigations whereby TMM modelling was applied to various thermo-mechanical processes in titanium alloys, predominantly Ti-6Al-4V, is provided in Table 4. This includes details of the process conditions, sub-models and validation techniques applied.

A comprehensive study was conducted by Ahn *et al.* [70] whereby residual stress and distortion was measured and predicted for fibre laser welding of Ti-6Al-4V; with additional microstructure prediction. Transformation plasticity and creep were assumed minimal and therefore not considered in the model. It was found that transformation induced volume change had a small influence on magnitude of residual stress and this was attributed to the similarities in unit cell volume between α and β phases; which can lead to associated strains an order of magnitude smaller than that exhibited in steels [164]. Additionally, a comparison between measured and predicted distortion, with and without consideration of ε_{ij}^{tv}, found that models which did not consider ε_{ij}^{tv} were more accurate. It was therefore suggested that distortion is more sensitive to phase transformation than residual stress itself. A particular explanation for the inaccuracies in distortion prediction where phase transformation was considered may be due to the omission of transformation induced plasticity in the model, as the accumulation of strain of a plastic nature may have caused notable plastic deformation, affecting distortion. As residual stress is elastic in nature, such plastic deformation would not be depicted within this data [6]. Both diffusional and martensitic transformations were modelled.

Teixeira *et al.* [53] considered quenching of Ti-17; an α+β alloy with similar characteristics to Ti-6Al-4V, from above the β-transus temperature. The majority of residual stress generation was attributed to thermal and visco-plastic strain components rather than being of microstructural origin. Transformation induced plasticity was considered using equations based on the Greenwood-Johnson effect; modified for Ti-17 alloy, and transformation induced volume changes were approximated as 0.2%; yet these components of strain were found to have a minimal effect on residual stress. Such findings are in agreement with arguments presented by Lindgren [165], especially considering the propensity for transformation induced plasticity to lead to mitigation rather than intensification of residual stress [89, 166]. However, the findings were not supported by experimental model validation; which could be explored as part of future work.

Lindgren *et al.* [69] considered metal deposition of Ti-6Al-4V whereby a coupled TMM model was used which incorporated the Babu physically based constitutive model for mechanical properties and the Kelly-Charles and Koistinen-Marburger models for microstructural evolution. However, transformation induced plasticity was not considered and the modelling of creep strain was not discussed [69]. Distortion measurement was conducted at two points, with one comparing well with simulated data, and some discrepancy for the other point. Although advanced microstructural modelling was conducted, no microstructural validation was presented for the case study material. Deviations from simulated data was attributed to the lack of high temperature constitutive data available from 1100-1600°C which is experienced during metal deposition. Thus, the model may be more accurate when applied to heat treatment as this is normally conducted below 1100°C [36].

Despite recent advances in residual stress measurement and the potential benefits of carrying out a number of complimentary measurements for through-thickness comparison, few have carried out such validation. Additionally, numerous authors [90, 94, 167] have utilised detailed modelling approaches, with little or no accompanying experimental validation of residual stress. Although this provides advancements in modelling capability, the accuracy of such models must be appropriately scrutinised in order to ensure model accuracy and determine the most, or least, significant contributors to total strain [52].

It can be noted in Table 4 that the creep strain component is not considered to the same extent as visco-plastic strain within mechanical sub-models. This may be partially due to the microstructural sensitivity of the stress relaxation response coupled with the high relaxation rates at elevated temperatures allowing for the assumption that complete stress relaxation takes place. On the other hand, this may be the case due to the comparative lack of fundamental studies of stress relaxation response in titanium alloys. By overlooking stress relaxation, this may lead to over-prediction of residual stress magnitudes.

Table 4: Summary of TMM based modelling studies of residual stress in titanium alloys.

Author	Alloy	Conditions	Metallurgical Model (ε_{met})				Thermal Model (ε_{th})		Mechanical Model (ε_{mech})			Validation Technique
			Type(s)	Phases Considered	Transformation Induced Plasticity (ε_{tr})	Transformation Induced Volume Change (ε_{tv})	Heat Transfer Coefficient	Thermal Strain (ε_{th})	Creep (ε_{cr})	Plasticity (ε_p)		
										Model	Strain Rate Dependence	
Lindgren *et al.* (2016) [69]	Ti-6Al-4V	DED	Kelly-Charles and KM	$\alpha_{gb}, \alpha_w, \alpha_m, \beta$	-	Incorporated in thermal model	-	(Macro) Thermal expansion	-	Babu	Yes	Distortion
Denlinger *et al.* (2014) [99]	Ti-6Al-4V	EBM	Not Modelled	-	-	Incorporated in thermal model	-	(Macro) Thermal expansion	Complete relaxation at 640°C	Tabular data	No	Hole drilling, distortion
Ahn *et al.* (2016) [70]	Ti-6Al-4V	Welding	Modified JMAK and KM	α, β, α_m	Assumed Negligible	From [33] unit cell volume based	Experimentally	JMatPro phase based	Assumed Negligible	Elastic-Plastic	No	XRD, Neutron Diffraction, Distortion
Cao *et al.* (2016) [19]	Ti-6Al-4V	EBM	Not Modelled	-	-	Incorporated in thermal model	-	(Macro) Thermal expansion	Complete relaxation at 640°C [99]	Elastic-plastic	No	Neutron diffraction, hole drilling
Xie *et al.*(2015) [72]	Ti-6Al-4V	EBW	Not Modelled	-	-	Incorporated in thermal model	-	(Macro) Thermal expansion	-	Elastic-plastic	No	Contour method
Teixeira *et al.* (2016) [53]	Ti17	Quench	JMAK	α, β, α_m	Greenwood and Johnson [92]	Assumed 0.2% [168]	-	Unit cell volume based	-	Elastic-Plastic	Yes	-
Song *et al.* (2015) [90]	TA15	Welding	JMAK and KM	α, β, α_m	Greenwood and Johnson [92]	Incorporated in thermal model	-	(Macro) Thermal expansion	-	Elastic-Plastic	No	Slitting
Ducato *et al.* (2013) [84]	Ti-6Al-4V	Forging	Simplified Avrami	α, β	-	-	-	-	-	JMatPro	Yes	-
Crespo et al. (2009) [94]	Ti-6Al-4V	DED	JMAK and KM	α, β, α_m	-	-	-	-	-	Semiatin	Yes	-
Heigel *et al.* (2015) [20]	Ti-6Al-4V	DED	Not Modelled	-	-	Incorporated in thermal model	-	(Macro) Thermal expansion	Complete relaxation at 640°C [99]	-	-	Hole Drilling
Deng *et al.* (2016) [169]	Ti-6Al-4V	Hot Stretch Bending	Not Modelled	-	-	-	-	-	Arrhenius equation	JC	Yes	Distortion
Bühr *et al.* (2018) [18]	Ti-6Al-4V	LFW	Not Modelled	-	-	Incorporated in thermal model	-	(Macro) Thermal Expansion	Complete relaxation above 800°C	Chen *et al.* [170] & Guo *et al.* [123]	No	Contour Method and Neutron Diffraction

4. Conclusions

Although a number of the aforementioned studies have made great developments towards the understanding of specific aspects and sub-models used in the TMM modelling of titanium alloys, few have attempted to unite all aspects of this state-of-the-art research for the prediction of residual stress evolution. It is therefore recommended that future TMM modelling endeavours involving the thermo-mechanical processing of Ti-6Al-4V consider all of these multifaceted areas to ensure the utmost scientific rigour. The following considerations were identified for future research:

- It should be ensured that thermal expansion coefficients and transformation induced volume change components are used accordingly based on their origin; macroscopic or lattice parameter based.
- Further investigation and initial experimental measurement of transformation induced plasticity in titanium alloys should be conducted, as the majority of previous studies were concentrated on steels.
- The stress relaxation behaviour of Ti-6Al-4V should be studied in more detail, particularly with regards to modelling efforts and the effect of microstructural differences on the stress relaxation response.
- Complimentary residual stress measurement techniques may be used for model validation; tailored to the material and region of interest.

Acknowledgements

The author is grateful for the guidance of Dr. S. Rahimi. This work was supported by the Engineering and Physical Sciences Research Council (EPSRC) grant (EP/1015698/1). The author would also like to thank TIMET and Aubert & Duval for their support on the project. The research was performed at the Advanced Forming Research Centre (AFRC), which receives partial financial support from the UK's High Value Manufacturing Catapult.

References

1. Lutjering G, Williams JC. Introduction. In: Derby B, editor. Titanium. 2 ed: Springer-Verlag Berlin Heidelberg; 2007. p. 1-15.
2. Mouritz A. Titanium Alloys for Aerospace Structures and Engines. In: Mouritz A, editor. Introduction to Aerospace Materials: Woodhead Publishing; 2012. p. 202-223.
3. Dieter GE. Fundamentals of Metalworking. Mechanical Metallurgy. 3 ed: McGraw-Hill; 1988. p. 557-559.
4. Hardin RA, Beckermann C, editors. Simulation of Heat Treatment Distortion. Proceedings of the 59th SFSA Technical and Operating Conferance; 2005; Chicago: Steel Founders' Society of America.
5. Turner R, Schroeder F, Ward RM, et al. The Importance of Materials Data and Modelling Parameters in an FE Simulation of Linear Friction Welding. Advances in Materials Science and Engineering. 2014. doi: 10.1155/2014/521937. PubMed PMID: WOS:000332563000001.
6. Withers PJ, Bhadeshia HKDH. Residual Stress. Part 2 - Nature and Origins. Materials Science and Technology. 2001 Apr;17(4):366-375. PubMed PMID: WOS:000168427800002.
7. Withers PJ, Bhadeshia H. Overview - Residual stress part 1 - Measurement techniques. Materials Science and Technology. 2001 Apr;17(4):355-365. PubMed PMID: WOS:000168427800001.
8. Brunel F, Brunel J-F, Dufrénoy P, et al. Prediction of the Initial Residual Stresses in Railway Wheels Induced by Manufacturing. Journal of Thermal Stresses. 2013 2013/01/02;36(1):37-55. doi: 10.1080/01495739.2012.720542.
9. MacKenzie DS, Lambert D. Effect of quenching variables on distortion and residual stresses. Heat Treating and Surface Engineering, Indiana, USA. 2003:184-191.
10. Robinson JS, Tanner DA, Truman CE. 50th Anniversary Article: The Origin and Management of Residual Stress in Heat-treatable Aluminium Alloys. Strain. 2014;50(3):185-207. doi: 10.1111/str.12091.
11. Maijer DM, Gao YX, Lee PD, et al. A through-process model of an A356 brake caliper for fatigue life prediction. Metallurgical and Materials Transactions A. 2004 2004//;35(10):3275-3288. doi: 10.1007/s11661-004-0070-3.
12. Tanner DA, Robinson JS. Residual stress prediction and determination in 7010 aluminum alloy forgings. Experimental Mechanics. 2000 2000//;40(1):75-82. doi: 10.1007/BF02327551.
13. Navalho D, Deus AM, Infante V, et al. Residual Stresses Due to Quenching in Aluminum Forging Parts for Aerospace Applications: Finite Element Analysis and Contour Method Measurement. 2012.
14. Dye D, Conlon KT, Reed RC. Characterization and modeling of quenching-induced residual stresses in the nickel-based superalloy IN718. Metallurgical and Materials Transactions A. 2004 2004//;35(6):1703-1713. doi: 10.1007/s11661-004-0079-7.
15. Rauer G, Kühhorn A, Springmann M. Residual Stress Modelling and Inverse Heat Transfer Coefficients Estimation of a Nickel-Based Superalloy Disc Forging. 2014 (45752):V006T22A009. doi: 10.1115/GT2014-25827.
16. Weiner JH, Huddleston JV. Transient and residual stresses in heat-treated cylinders. Journal of Applied Mechanics. 1959;26(1):31-39.
17. Glavicic MG, Furrer DU, Shen G. A Rolls-Royce Corporation industrial perspective of titanium process modelling and optimization: current capabilities

and future needs. Journal of Strain Analysis for Engineering Design. 2010;45(5):329-335. doi: 10.1243/03093247jsa577. PubMed PMID: WOS:000279779900002.
18. Bühr C, Ahmad B, Colegrove PA, et al. Prediction of residual stress within linear friction welds using a computationally efficient modelling approach. Materials & Design. 2018 2018/02/05/;139:222-233. doi: https://doi.org/10.1016/j.matdes.2017.11.013.
19. Cao J, Gharghouri MA, Nash P. Finite-element analysis and experimental validation of thermal residual stress and distortion in electron beam additive manufactured Ti-6Al-4V build plates [Article]. Journal of Materials Processing Technology. 2016 Nov;237:409-419. doi: 10.1016/j.jmatprotec.2016.06.032. PubMed PMID: WOS:000381323500038; English.
20. Heigel JC, Michaleris P, Reutzel EW. Thermo-mechanical model development and validation of directed energy deposition additive manufacturing of Ti–6Al–4V. Additive Manufacturing. 2015 2015/01/01/;5:9-19. doi: https://doi.org/10.1016/j.addma.2014.10.003.
21. Donachie MJ. Titanium: A Technical Guide, 2nd Edition. ASM International; 2000.
22. Veiga C, Devim JP, Loureiro AJR. Properties and Applications of Titanium Alloys: A Brief Review. Reviews on Advanced Materials Science. 2012 Dec;32(2):133-148. PubMed PMID: WOS:000313153800005.
23. Burgers WG. On the process of transition of the cubic-body-centered modification into the hexagonal-close-packed modification of zirconium. Physica. 1934;1(7-12):561-586.
24. Sargent GA, Kinsel KT, Pilchak AL, et al. Variant selection during cooling after beta annealing of Ti-6Al-4V ingot material. Metallurgical and Materials Transactions A. 2012;43(10):3570-3585.
25. Obasi GC, Moat RJ, Leo Prakash DG, et al. In situ neutron diffraction study of texture evolution and variant selection during the α→β→α phase transformation in Ti–6Al–4V. Acta Materialia. 2012 2012/12/01/;60(20):7169-7182. doi: https://doi.org/10.1016/j.actamat.2012.09.026.
26. ASTM International. ASTM B348-13 Standard Specification for Titanium and Titanium Alloy Bars and Billets. West Conshohocken, PA.
27. Sieniawski J, Ziaja W, Kubiak K, et al. Microstructure and Mechanical Properties of High Strength Two-Phase Titanium Alloys. In: Sieniawski J, Ziaja W, editors. Titanium Alloys - Advances in Properties Control. Rijeka: InTech; 2013. p. Ch. 04.
28. Ghosh G. Thermodynamic and kinetic modeling of the Cr-Ti-V system. Journal of phase equilibria. 2002;23(4):310.
29. Witusiewicz VT, Bondar AA, Hecht U, et al. The Al–B–Nb–Ti system: III. Thermodynamic re-evaluation of the constituent binary system Al–Ti. Journal of alloys and compounds. 2008;465(1-2):64-77.
30. Peters M, Kumpfert J, Ward CH, et al. Titanium alloys for aerospace applications. Advanced Engineering Materials. 2003;5(6):419-427.
31. Elmer JW, Palmer TA, Babu SS, et al. Low temperature relaxation of residual stress in Ti–6Al–4V. Scripta Materialia. 2005 5//;52(10):1051-1056. doi: http://dx.doi.org/10.1016/j.scriptamat.2005.01.021.
32. Malinov S, Sha W, Guo Z, et al. Synchrotron X-ray diffraction study of the phase transformations in titanium alloys. Materials Characterization. 2002;48(4):279-295.

33. Elmer JW, Palmer TA, Babu SS, et al. In situ observations of lattice expansion and transformation rates of α and β phases in Ti–6Al–4V. Materials Science and Engineering: A. 2005 2005/01/25/;391(1):104-113. doi: http://dx.doi.org/10.1016/j.msea.2004.08.084.
34. Kherrouba N, Bouabdallah M, Badji R, et al. Beta to alpha transformation kinetics and microstructure of Ti-6Al-4V alloy during continuous cooling. Materials Chemistry and Physics. 2016 2016/09/15/;181:462-469. doi: https://doi.org/10.1016/j.matchemphys.2016.06.082.
35. Lütjering G. Influence of processing on microstructure and mechanical properties of (α+ β) titanium alloys. Materials Science and Engineering: A. 1998;243(1-2):32-45.
36. Alpha + Beta Alloys. In: Lütjering G, Williams JC, editors. Titanium. Berlin, Heidelberg: Springer Berlin Heidelberg; 2007. p. 203-258.
37. Gil FJ, Ginebra MP, Manero JM, et al. Formation of α-Widmanstätten structure: effects of grain size and cooling rate on the Widmanstätten morphologies and on the mechanical properties in Ti6Al4V alloy. Journal of Alloys and Compounds. 2001 2001/11/14/;329(1):142-152. doi: https://doi.org/10.1016/S0925-8388(01)01571-7.
38. Filip R, Kubiak K, Ziaja W, et al. The effect of microstructure on the mechanical properties of two-phase titanium alloys. Journal of Materials Processing Technology. 2003 2003/02/01/;133(1):84-89. doi: http://dx.doi.org/10.1016/S0924-0136(02)00248-0.
39. Ma K, Goetz R, Srivatsa SK. Modeling of residual stress and machining distortion in aerospace components. ASM Handbook, Metals Process Simulation B. 2010;22:386-407.
40. Welsch G, Boyer R, Collings EW. Materials Properties Handbook: Titanium Alloys. ASM International; 1993. (Materials properties handbook).
41. Reed-Hill RE, Abbaschian R. Physical metallurgy principles. Brooks/Cole Engineering Division Monterey, Calif, USA; 1973.
42. Semiatin SL, Knisley SL, Fagin PN, et al. Microstructure evolution during alpha-beta heat treatment of Ti-6Al-4V. Metallurgical and Materials Transactions A. 2003 2003//;34(10):2377-2386. doi: 10.1007/s11661-003-0300-0.
43. Ahmed T, Rack HJ. Phase transformations during cooling in α+β titanium alloys. Materials Science and Engineering: A. 1998 1998/03/15/;243(1):206-211. doi: http://dx.doi.org/10.1016/S0921-5093(97)00802-2.
44. Handbook ASM. vol. 4B: Steel Heat Treating Technologies, Basics of Distortion and Stress Generation During Heat Treatment. ASM International. 2014:339-354.
45. Xie P, Zhao H, Wu B, et al. Evaluation of Residual Stresses Relaxation by Post Weld Heat Treatment Using Contour Method and X-ray Diffraction Method. Experimental Mechanics. 2015 Sep;55(7):1329-1337. doi: 10.1007/s11340-015-0040-2. PubMed PMID: WOS:000361138000011.
46. Zhang X-Y, Fang G, Leeflang S, et al. Effect of subtransus heat treatment on the microstructure and mechanical properties of additively manufactured Ti-6Al-4V alloy. Journal of Alloys and Compounds. 2018;735:1562-1575.
47. Wang Z, Stoica AD, Ma D, et al. Stress relaxation behavior and mechanisms in Ti-6Al-4V determined via in situ neutron diffraction: Application to additive manufacturing. Materials Science and Engineering: A. 2017

2017/11/07/;707(Supplement C):585-592. doi: https://doi.org/10.1016/j.msea.2017.09.071.
48. Ter Haar GM, Becker TH. Selective Laser Melting Produced Ti-6Al-4V: Post-Process Heat Treatments to Achieve Superior Tensile Properties. Materials. 2018;11(1):146.
49. Hönnige JR, Colegrove PA, Ahmad B, et al. Residual stress and texture control in Ti-6Al-4V wire+ arc additively manufactured intersections by stress relief and rolling. Materials & Design. 2018;150:193-205.
50. Rohde J, Jeppsson A. Literature review of heat treatment simulations with respect to phase transformation, residual stresses and distortion. Scandinavian Journal of Metallurgy. 2000;29(2):47-62. doi: 10.1034/j.1600-0692.2000.d01-6.x.
51. Simsir C, Gür CH. A Review on Modeling and Simulation of Quenching. Journal of ASTM International(JAI). 2010;1523:117-156.
52. Bhadeshia H. Mathematical models in materials science. Materials Science and Technology. 2008;24(2):128-136.
53. Teixeira J, Denand B, Aeby-Gautier E, et al. Simulation of coupled temperature, microstructure and internal stresses evolutions during quenching of a β-metastable titanium alloy. Materials Science and Engineering: A. 2016;651:615-625.
54. Ahn J. Experimental characterisation and numerical simulation of fibre laser welding of AA 2024-T3 and Ti-6Al-4V. 2016.
55. Schuh C, Dunand DC. Non-isothermal transformation-mismatch plasticity: modeling and experiments on Ti–6Al–4V. Acta Materialia. 2001 2001/01/22/;49(2):199-210. doi: https://doi.org/10.1016/S1359-6454(00)00318-9.
56. Xiao B, Li K, Wang Q, et al. Numerical Simulation and Experimental Validation of Residual Stresses in Water-Quenched Aluminum Alloy Castings. Journal of Materials Engineering and Performance. 2011 2011//;20(9):1648-1657. doi: 10.1007/s11665-011-9866-7.
57. Xie J, Oancea V, Hurtado J. Phase Transformations in Metals during Additive Manufacturing Processes. NAFEMS World Congress 2017; Stockholm2017.
58. Ho A, Zhao H, Fellowes JW, et al. On the origin of microstructural banding in Ti-6Al4V wire-arc based high deposition rate additive manufacturing. Acta Materialia. 2019;166:306-323.
59. Knoedel P, Gkatzogiannis S, Ummenhofer T. Practical aspects of welding residual stress simulation. Journal of Constructional Steel Research. 2017 2017/05/01/;132:83-96. doi: https://doi.org/10.1016/j.jcsr.2017.01.010.
60. Coules HE. Contemporary Approaches to Reducing Weld Induced Residual Stress. Materials Science and Technology. 2013;29(1):4-18.
61. Denis S, Archambault P, Gautier E, et al. Prediction of residual stress and distortion of ferrous and non-ferrous metals: Current status and future developments. Journal of Materials Engineering and Performance. 2002 2002//;11(1):92-102. doi: 10.1007/s11665-002-0014-2.
62. Majorek A, Scholtes B, Muller H, et al. The influence of heat transfer on the development of stresses, residual stresses and distortions in martensitically hardened SAE 1045 and SAE 4140. Quenching and Distortion Control. 1992:171-179.

63. Majorek A. Der Einfluß des Wärmeübergangs auf die Eigenspannungs- und Verzugsausbildung beim Abschrecken von Stahlzylindern in verdampfenden Flüssigkeiten. PhD Thesis. 1996;Karlsruhe University.
64. Pollard JD, Rahimi S, Watford A, et al. The determination of residual stress in extruded Ti-6Al-4V by contour method and finite element analysis. 2016.
65. Bhatti AA, Barsoum Z, Murakawa H, et al. Influence of thermo-mechanical material properties of different steel grades on welding residual stresses and angular distortion. Materials & Design (1980-2015). 2015 2015/01/01/;65:878-889. doi: http://dx.doi.org/10.1016/j.matdes.2014.10.019.
66. Asserin O, Loredo A, Petelet M, et al. Global sensitivity analysis in welding simulations—What are the material data you really need? Finite Elements in Analysis and Design. 2011 2011/09/01/;47(9):1004-1016. doi: http://dx.doi.org/10.1016/j.finel.2011.03.016.
67. Zhu XK, Chao YJ. Effects of temperature-dependent material properties on welding simulation. Computers & Structures. 2002;80(11):967-976.
68. James JD, Spittle JA, Brown SGR, et al. A review of measurement techniques for the thermal expansion coefficient of metals and alloys at elevated temperatures. Measurement Science and Technology. 2001;12(3):R1.
69. Lindgren L-E, Lundbäck A, Fisk M, et al. Simulation of additive manufacturing using coupled constitutive and microstructure models. Additive Manufacturing. 2016 2016/10/01/;12:144-158. doi: http://dx.doi.org/10.1016/j.addma.2016.05.005.
70. Ahn J, He E, Chen L, et al. Prediction and measurement of residual stresses and distortions in fibre laser welded Ti-6Al-4V considering phase transformation. Materials & Design. 2017 Feb;115:441-457. doi: 10.1016/j.matdes.2016.11.078. PubMed PMID: WOS:000390654500047.
71. Baruah M, Bag S. Influence of heat input in microwelding of titanium alloy by micro plasma arc. Journal of Materials Processing Technology. 2016;231:100-112.
72. Xie P, Zhao HY, Wu B, et al. Using Finite Element and Contour Method to Evaluate Residual Stress in Thick Ti-6Al-4V Alloy Welded by Electron Beam Welding. Acta Metallurgica Sinica-English Letters. 2015 Jul;28(7):922-930. doi: 10.1007/s40195-015-0276-y. PubMed PMID: WOS:000358553000014.
73. Belskaya EA. Emissivity and electrical resistivity of titanium alloys with aluminum and vanadium. High Temperature. 2012;50(4):475-478.
74. Powell RW, Tye RP. The thermal and electrical conductivity of titanium and its alloys. Journal of the less Common Metals. 1961;3(3):226-233.
75. Irwin J, Reutzel EW, Michaleris P, et al. Predicting microstructure from thermal history during additive manufacturing for Ti-6Al-4V. Journal of Manufacturing Science and Engineering. 2016;138(11):111007.
76. Kelly SM. Thermal and microstructure modeling of metal deposition processes with application to Ti-6Al-4V. 2004.
77. Wang YZ, Ma N, Chen Q, et al. Predicting phase equilibrium, phase transformation, and microstructure evolution in titanium alloys. Jom. 2005;57(9):32-39.
78. Salsi E, Chiumenti M, Cervera M. Modeling of Microstructure Evolution of Ti6Al4V for Additive Manufacturing. Metals. 2018;8(8):633.
79. Malinov S, Markovsky P, Sha W, et al. Resistivity study and computer modelling of the isothermal transformation kinetics of Ti–6Al–4V and Ti–6Al–

2Sn–4Zr–2Mo–0.08 Si alloys. Journal of Alloys and Compounds. 2001;314(1-2):181-192.
80. Malinov S, Guo Z, Sha W, et al. Differential scanning calorimetry study and computer modeling of β⇒ α phase transformation in a Ti-6Al-4V alloy. Metallurgical and Materials Transactions A. 2001;32(4):879-887.
81. Saunders N, Guo UKZ, Li X, et al. Using JMatPro to model materials properties and behavior. Jom. 2003;55(12):60-65.
82. Charles Murgau C, Pederson R, Lindgren L-E. A model for Ti–6Al–4V microstructure evolution for arbitrary temperature changes. Modelling and Simulation in Materials Science and Engineering. 2012;20(5):055006.
83. Charles Murgau C. Microstructure Model for Ti-6Al-4V used in Simulation of Additive Manufacturing. 2016.
84. Ducato A, Fratini L, Micari F. Prediction of phase transformation of Ti-6Al-4V titanium alloy during hot-forging processes using a numerical model. Proceedings of the Institution of Mechanical Engineers, Part L: Journal of Materials: Design and Applications. 2013 2014/07/01;228(3):154-159. doi: 10.1177/1464420713477344.
85. Elmer JW, Palmer TA, Babu SS, et al. Phase transformation dynamics during welding of Ti–6Al–4V. Journal of applied physics. 2004;95(12):8327-8339.
86. Vander Voort GF. Atlas of time-temperature diagrams for irons and steels. ASM international; 1991.
87. Koistinen DP, Marburger RE. A general equation prescribing the extent of the austenite-martensite transformation in pure iron-carbon alloys and plain carbon steels. Acta Metallurgica. 1959 1959/01/01/;7(1):59-60. doi: https://doi.org/10.1016/0001-6160(59)90170-1.
88. Fischer FD, Reisner G, Werner E, et al. A new view on transformation induced plasticity (TRIP). International Journal of Plasticity. 2000 2000/06/01/;16(7):723-748. doi: https://doi.org/10.1016/S0749-6419(99)00078-9.
89. O'Meara N. Developing material models for use in finite element predictions of residual stresses in ferritic steel welds. 2016.
90. Song KJ, Wei YH, Dong ZB, et al. Constitutive model coupled with mechanical effect of volume change and transformation induced plasticity during solid phase transformation for TA15 alloy welding. Applied Mathematical Modelling. 2015 2015/04/01/;39(7):2064-2080. doi: http://dx.doi.org/10.1016/j.apm.2014.10.020.
91. Magee CL, Paxton HW. Transformation Kinetics, Microplasticity, and Aging of Martensite in Fe-31 Ni. CARNEGIE INST OF TECH PITTSBURGH PA; 1966.
92. Greenwood GW, Johnson RH. The deformation of metals under small stresses during phase transformations. Proc R Soc Lond A. 1965;283(1394):403-422.
93. Dalgic M, Löwisch G. Transformation plasticity at different phase transformations of bearing steel. Materialwissenschaft und Werkstofftechnik: Entwicklung, Fertigung, Prüfung, Eigenschaften und Anwendungen technischer Werkstoffe. 2006;37(1):122-127.
94. Crespo A, Deus A, Vilar R, editors. Modeling of phase transformations and internal stresses in laser powder deposition2009
2009: International Society for Optics and Photonics.
95. Bruno G, Dunn BD. The precise measurement of Ti6Al4V microscopic elastic constants by means of neutron diffraction. Measurement Science and Technology. 1997;8(11):1244.

96. Rahimi S, King M, Dumont C. Stress relaxation behaviour in IN718 nickel based superalloy during ageing heat treatments. Materials Science and Engineering: A. 2017 2017/12/21/;708:563-573. doi: https://doi.org/10.1016/j.msea.2017.09.116.
97. Konkova T, Rahimi S, Mironov S, et al. Effect of strain level on the evolution of microstructure in a recently developed AD730 nickel based superalloy during hot forging. Materials Characterization. 2018 2018/05/01/;139:437-445. doi: https://doi.org/10.1016/j.matchar.2018.03.027.
98. Babu B. Physically based model for plasticity and creep of Ti-6Al-4V. 2008.
99. Denlinger ER, Heigel JC, Michaleris P. Residual stress and distortion modeling of electron beam direct manufacturing Ti-6Al-4V. Proceedings of the Institution of Mechanical Engineers, Part B: Journal of Engineering Manufacture. 2014 2015/10/01;229(10):1803-1813. doi: 10.1177/0954405414539494.
100. Alabort E, Putman D, Reed RC. Superplasticity in Ti-6Al-4V: Characterisation, modelling and applications. Acta Materialia. 2015 Aug;95:428-442. doi: 10.1016/j.actamat.2015.04.056. PubMed PMID: WOS:000358626200044.
101. Johnson GR. A constitutive model and data for materials subjected to large strains, high strain rates, and high temperatures. Proc 7th Inf Sympo Ballistics. 1983:541-547.
102. Johnson GR, Cook WH. Fracture characteristics of three metals subjected to various strains, strain rates, temperatures and pressures. Engineering fracture mechanics. 1985;21(1):31-48.
103. Yin DQ, Wang DP, Li WH, et al. Development of a new 3D model for the prediction of residual stress and fracture behaviour in Ti-6Al-4V after ultrasonic peening treatment [Article]. Journal of Materials Processing Technology. 2017 Sep;247:29-39. doi: 10.1016/j.jmatprotec.2017.03.033. PubMed PMID: WOS:000403133400004; English.
104. Kotkunde N, Deole AD, Gupta AK, et al. Comparative study of constitutive modeling for Ti–6Al–4V alloy at low strain rates and elevated temperatures. Materials & Design. 2014 3//;55:999-1005. doi: http://dx.doi.org/10.1016/j.matdes.2013.10.089.
105. Lee W-S, Lin C-F. High-temperature deformation behaviour of Ti6Al4V alloy evaluated by high strain-rate compression tests. Journal of Materials Processing Technology. 1998 1998/03/01/;75(1):127-136. doi: https://doi.org/10.1016/S0924-0136(97)00302-6.
106. Picu RC, Majorell A. Mechanical behavior of Ti–6Al–4V at high and moderate temperatures—Part II: constitutive modeling. Materials Science and Engineering: A. 2002 3/31/;326(2):306-316. doi: http://dx.doi.org/10.1016/S0921-5093(01)01508-8.
107. Seo S, Min O, Yang H. Constitutive equation for Ti–6Al–4V at high temperatures measured using the SHPB technique. International Journal of Impact Engineering. 2005 2005/07/01/;31(6):735-754. doi: https://doi.org/10.1016/j.ijimpeng.2004.04.010.
108. Fergani O, Atmani Z, Zenasni M, et al. Physics-Based Model to Predict Forces and Chip Morphology in the Machining of a Ti-6Al-4V Alloys for Aeronautical Applications. Procedia Manufacturing. 2016;6:53-62.
109. Semiatin SL, Montheillet F, Shen G, et al. Self-consistent modeling of the flow behavior of wrought alpha/beta titanium alloys under isothermal and nonisothermal hot-working conditions. Metallurgical and Materials Transactions A. 2002;33(8):2719-2727.

110. Babu B, Lindgren L-E. Dislocation density based model for plastic deformation and globularization of Ti-6Al-4V. International Journal of Plasticity. 2013 11//;50:94-108. doi: http://dx.doi.org/10.1016/j.ijplas.2013.04.003.
111. Souza PM, Beladi H, Singh R, et al. Constitutive analysis of hot deformation behavior of a Ti6Al4V alloy using physical based model. Materials Science and Engineering a-Structural Materials Properties Microstructure and Processing. 2015 Nov;648:265-273. doi: 10.1016/j.msea.2015.09.055. PubMed PMID: WOS:000363820700035.
112. Fan XG, Yang H. Internal-state-variable based self-consistent constitutive modeling for hot working of two-phase titanium alloys coupling microstructure evolution. International Journal of Plasticity. 2011 2011/11/01/;27(11):1833-1852. doi: https://doi.org/10.1016/j.ijplas.2011.05.008.
113. Conrad H. Effect of interstitial solutes on the strength and ductility of titanium. Progress in Materials Science. 1981;26(2-4):123-403.
114. Mecking H, Kocks UF. Kinetics of flow and strain-hardening. Acta Metallurgica. 1981 1981/11/01/;29(11):1865-1875. doi: https://doi.org/10.1016/0001-6160(81)90112-7.
115. Follansbee PS, Gray GT. An analysis of the low temperature, low and high strain-rate deformation of Ti− 6Al− 4V. Metallurgical Transactions A. 1989;20(5):863-874.
116. Seshacharyulu T, Medeiros SC, Frazier WG, et al. Microstructural mechanisms during hot working of commercial grade Ti–6Al–4V with lamellar starting structure. Materials Science and Engineering: A. 2002 2002/02/28/;325(1):112-125. doi: https://doi.org/10.1016/S0921-5093(01)01448-4.
117. Gao P, Yang H, Fan X, et al. Unified modeling of flow softening and globularization for hot working of two-phase titanium alloy with a lamellar colony microstructure. Journal of Alloys and Compounds. 2014 2014/07/05/;600:78-83. doi: https://doi.org/10.1016/j.jallcom.2014.02.110.
118. Majorell A, Srivatsa S, Picu RC. Mechanical behavior of Ti–6Al–4V at high and moderate temperatures—Part I: Experimental results. Materials Science and Engineering: A. 2002 3/31/;326(2):297-305. doi: http://dx.doi.org/10.1016/S0921-5093(01)01507-6.
119. De Meester B, Döner M, Conrad H. Deformation kinetics of the Ti-6Al-4V alloy at low temperatures. Metallurgical Transactions A. 1975;6(1):65-75.
120. International Conference on T, Jaffee RI, Burte HM, et al., editors. Titanium science and technology; proceedings1973; New York: Plenum Press.
121. Blenkinsop PA, Evans WJ, Flower HM. Titanium'95: science and technology: proceedings of the Eighth World Conference on Titanium held at the International Convention Centre, Birmingham, UK, 22-26 October 1995. Vol. 3. Institute of Materials; 1996.
122. Lütjering G, Zwicker U, Bunk W. Titanium Science and Technology: Proceedings of the Fifth International Conference on Titanium, Congress-Center, Munich, FRG, September 10-14, 1984. DGM; 1985. (Titanium Science and Technology: Proceedings of the Fifth International Conference on Titanium, Congress-Center, Munich, FRG, September 10-14, 1984).
123. Guo Z, Saunders N, Schillé JP, et al., editors. Modelling high temperature flow stress curves of titanium alloys2008.
124. Warwick JLW, Coakley J, Raghunathan SL, et al. Effect of texture on load partitioning in Ti-6Al-4V. Acta Materialia. 2012 2012/06/01/;60(10):4117-4127. doi: http://dx.doi.org/10.1016/j.actamat.2012.03.039.

125. Prasad Y, Rao KP, Sasidhar S. Hot working guide: a compendium of processing maps. ASM international; 2015.
126. Kumar A, Srivastava A, Goel N, et al. Creep Mechanisms vis-à-vis Power Law vs. Grain Boundary Sliding in α-β Titanium Alloys for Physics Based Prognostics.
127. Kim JH, Semiatin SL, Lee CS. Constitutive analysis of the high-temperature deformation of Ti–6Al–4V with a transformed microstructure. Acta Materialia. 2003 10/20/;51(18):5613-5626. doi: http://dx.doi.org/10.1016/S1359-6454(03)00426-9.
128. Kim JH, Semiatin SL, Lee CS. High-temperature deformation and grain-boundary characteristics of titanium alloys with an equiaxed microstructure. Materials Science and Engineering: A. 2008 6/25/;485(1–2):601-612. doi: http://dx.doi.org/10.1016/j.msea.2007.08.027.
129. Lee T, Kim JH, Semiatin SL, et al. Internal-variable analysis of high-temperature deformation behavior of Ti–6Al–4V: A comparative study of the strain-rate-jump and load-relaxation tests. Materials Science and Engineering: A. 2013 2/1/;562:180-189. doi: http://dx.doi.org/10.1016/j.msea.2012.11.023.
130. Yan G, Crivoi A, Sun Y, et al. An Arrhenius equation-based model to predict the residual stress relief of post weld heat treatment of Ti-6Al-4V plate. Journal of Manufacturing Processes. 2018 2018/04/01/;32:763-772. doi: https://doi.org/10.1016/j.jmapro.2018.04.004.
131. Kim JH, Semiatin SL, Lee CS. Constitutive analysis of the high-temperature deformation mechanisms of Ti-6Al-4V and Ti-6.85Al-1.6V alloys. Materials Science and Engineering a-Structural Materials Properties Microstructure and Processing. 2005 Mar;394(1-2):366-375. doi: 10.1016/j.msea.2004.11.061. PubMed PMID: WOS:000228069000043.
132. Alabort E, Kontis P, Barba D, et al. On the mechanisms of superplasticity in Ti–6Al–4V. Acta Materialia. 2016 2/15/;105:449-463. doi: http://dx.doi.org/10.1016/j.actamat.2015.12.003.
133. American Society of Mechanical Engineers, editor Guide for verification and validation in computational solid mechanics2006: ASME.
134. Easton D, Wood J, Rahimi S, et al. Residual Stress Generation in Brazed Tungsten Dissimilar Joints. IEEE Transactions on Plasma Science. 2016 Sep;44(9):1625-1630. doi: 10.1109/tps.2016.2565205. PubMed PMID: WOS:000384231500025.
135. Withers PJ. Residual stress and its role in failure. Reports on Progress in Physics. 2007 Dec;70(12):2211-2264. doi: 10.1088/0034-4885/70/12/r04. PubMed PMID: WOS:000252745700004.
136. Ahmad B, Fitzpatrick ME. Minimization and Mitigation of Wire EDM Cutting Errors in the Application of the Contour Method of Residual Stress Measurement [Article]. Metallurgical and Materials Transactions a-Physical Metallurgy and Materials Science. 2016 Jan;47A(1):301-313. doi: 10.1007/s11661-015-3231-7. PubMed PMID: WOS:000367468100031; English.
137. Fry AT. A Review of Residual Stress Measurement Methods - A Guide to Technique Selection. NPL Report MATC (A) 04; 2001.
138. Rossini NS, Dassisti M, Benyounis KY, et al. Methods of measuring residual stresses in components [Review]. Materials & Design. 2012 Mar;35:572-588. doi: 10.1016/j.matdes.2011.08.022. PubMed PMID: WOS:000301578700070; English.

139. Schajer GS, Ruud CO. Overview of Residual Stresses and Their Measurement. Practical Residual Stress Measurement Methods: John Wiley & Sons, Ltd; 2013. p. 1-27.
140. Sticchi M, Schnubel D, Kashaev N, et al. Review of Residual Stress Modification Techniques for Extending the Fatigue Life of Metallic Aircraft Components. Applied Mechanics Reviews. 2015 Jan;67(1). doi: 10.1115/1.4028160. PubMed PMID: WOS:000360284600001.
141. Withers PJ, Turski M, Edwards L, et al. Recent advances in residual stress measurement [Article]. International Journal of Pressure Vessels and Piping. 2008 Mar;85(3):118-127. doi: 10.1016/j.ijpvp.2007.10.007. PubMed PMID: WOS:000255536500002; English.
142. Benghalia G, Rahimi S, Wood J, et al. Multiscale Measurements of Residual Stress in a Low-Alloy Carbon Steel Weld Clad with IN625 Superalloy. Materials Performance and Characterization. 2018;7(4).
143. Inoue T, Wang Z-G, Miyao K, editors. Quenching stress of carburized steel gear wheel1989: Springer.
144. Steinzig M, Takahashi T. Residual stress measurement using the hole drilling method and laser speckle interferometry part IV: measurement accuracy. Experimental Techniques. 2003;27(6):59-63.
145. Prime MB, DeWald AT. The Contour Method. Practical Residual Stress Measurement Methods: John Wiley & Sons, Ltd; 2013. p. 109-138.
146. Withers PJ. Depth capabilities of neutron and synchrotron diffraction strain measurement instruments. II. Practical implications. Journal of applied crystallography. 2004;37(4):607-612.
147. Santisteban JR, Daymond MR, James JA, et al. ENGIN-X: a third-generation neutron strain scanner. Journal of Applied Crystallography. 2006;39(6):812-825.
148. Zhang L, Feng X, Li Z, et al. FEM simulation and experimental study on the quenching residual stress of aluminum alloy 2024. Proceedings of the Institution of Mechanical Engineers, Part B: Journal of Engineering Manufacture. 2013 2013/07/01;227(7):954-964. doi: 10.1177/0954405412465232.
149. Deleuze C, Barrallier L, Fabre A, et al. Microstructure characterisation of biphasic titanium alloy Ti–10V–2Fe–3Al and effects induced by heterogeneities on X-ray diffraction peak's broadening. Materials Science and Technology. 2011;27(10):1574-1581.
150. Rae W, Lomas Z, Jackson M, et al. Measurements of residual stress and microstructural evolution in electron beam welded Ti-6Al-4V using multiple techniques. Materials Characterization. 2017;132:10-19.
151. Rae W, Rahimi S. Evolution of Microstructure and Residual Stress in Hot Rolled Ti-6Al-4V Plates Subjected to Different Heat Treatment Conditions. Residual Stresses 2018: ECRS-10. 2018;6:171.
152. Mehdi B, Badji R, Ji V, et al. Microstructure and residual stresses in Ti-6Al-4V alloy pulsed and unpulsed TIG welds. Journal of Materials Processing Technology. 2016 May;231:441-448. doi: 10.1016/j.jmatprotec.2016.01.018. PubMed PMID: WOS:000372382900045.
153. Flowers Jr JW, O'Brien KC, McEleney PC. Elastic constants of alpha-titanium single crystals at 25 C. Journal of the Less Common Metals. 1964;7(5):393-395.
154. Stapleton AM, Raghunathan SL, Bantounas I, et al. Evolution of lattice strain in Ti–6Al–4V during tensile loading at room temperature. Acta Materialia. 2008;56(20):6186-6196.

155. Liu Y, Qin S, Hao Q, et al. Finite Element Simulation and Experimental Verification of Internal Stress of Quenched AISI 4140 Cylinders. Metallurgical and Materials Transactions A. 2017 2017//;48(3):1402-1413. doi: 10.1007/s11661-016-3916-6.
156. Leggatt RH, Smith DJ, Smith SD, et al. Development and experimental validation of the deep hole method for residual stress measurement. The Journal of Strain Analysis for Engineering Design. 1996;31(3):177-186.
157. Hosseinzadeh Ffhoau, Hossain S, Truman CE, et al. Measurement and Prediction of Residual Stresses in Quenched Stainless Steel Components [Article]. Experimental Mechanics. 2014 09//;54(7):1151-1162. doi: 10.1007/s11340-014-9890-2. PubMed PMID: 97370579.
158. Zheng G, Hossain S, Kingston E, et al. An optimisation study of the modified deep-hole drilling technique using finite element analyses applied to a stainless steel ring welded circular disc. International Journal of Solids and Structures. 2017 2017/07/01/;118-119:146-166. doi: https://doi.org/10.1016/j.ijsolstr.2017.04.008.
159. Rist MA, James JA, Tin S, et al. Residual stresses in a quenched superalloy turbine disc: measurements and modeling. Metallurgical and Materials Transactions A. 2006;37(2):459-467.
160. Pagliaro P, Prime MB, Robinson JS, et al. Measuring Inaccessible Residual Stresses Using Multiple Methods and Superposition. Experimental Mechanics. 2011 Sep;51(7):1123-1134. doi: 10.1007/s11340-010-9424-5. PubMed PMID: WOS:000293552900010.
161. Pagliaro P, Prime MB, Swenson H, et al. Measuring Multiple Residual-Stress Components using the Contour Method and Multiple Cuts [Article]. Experimental Mechanics. 2010 Feb;50(2):187-194. doi: 10.1007/s11340-009-9280-3. PubMed PMID: WOS:000274399500005; English.
162. Tsivoulas D, da Fonseca JQ, Tuffs M, et al. Effects of flow forming parameters on the development of residual stresses in Cr-Mo-V steel tubes [Article]. Materials Science and Engineering a-Structural Materials Properties Microstructure and Processing. 2015 Jan;624:193-202. doi: 10.1016/j.msea.2014.11.068. PubMed PMID: WOS:000348892100024; English.
163. Conroy B, Traoré Y, Paddea S, et al. Application of multiple residual stress determination methods to coarse-grained biomedical implant castings. Materials Science and Technology. 2017;33(10):1231-1251.
164. Szkliniarz W, Smołka G. Analysis of volume effects of phase transformation in titanium alloys. Journal of Materials Processing Technology. 1995 1995/08/01/;53(1):413-422. doi: http://dx.doi.org/10.1016/0924-0136(95)01998-T.
165. Lindgren L-E. Finite element modeling and simulation of welding part 1: increased complexity. Journal of thermal stresses. 2001;24(2):141-192.
166. Hoang H, Barbe F, Quey R, et al. FE determination of the plasticity induced during diffusive transformation in the case of nucleation at random locations and instants. Computational Materials Science. 2008;43(1):101-107.
167. Ducato A, Fratini L, Micari F, editors. Coupled thermo-mechanical-metallurgical analysis of an hot forging process of titanium alloy2013: Trans Tech Publ.
168. Teixeira J. Études expérimentales et modélisation des évolutions microstructurales au cours des traitements thermiques post forgeage dans l'alliage de titane Ti17. 2005.

169. Deng TS, Li DS, Li XQ, et al. Material characterization, constitutive modeling and validation in hot stretch bending of Ti-6Al-4V profile. Proceedings of the Institution of Mechanical Engineers Part B-Journal of Engineering Manufacture. 2016 Mar;230(3):505-516. doi: 10.1177/0954405414557371. PubMed PMID: WOS:000372897700011.
170. Chen G, Ren C, Qin X, et al. Temperature dependent work hardening in Ti–6Al–4V alloy over large temperature and strain rate ranges: Experiments and constitutive modeling. Materials & Design. 2015 10/15/;83:598-610. doi: http://dx.doi.org/10.1016/j.matdes.2015.06.048.